

# A CURRICULUM VIEW OF ROBUST LOSS FUNCTIONS

Zebin Ou<sup>1\*</sup> & Yue Zhang<sup>2</sup>

<sup>1</sup>Zhihu Inc., <sup>2</sup>School of Engineering, Westlake University  
ouzebin@zhihu.com, yuezhang@westlake.edu.cn

## ABSTRACT

Robust loss functions are designed to combat the adverse impacts of label noise, whose robustness is typically supported by theoretical bounds agnostic to the training dynamics. However, these bounds may fail to characterize the empirical performance as it remains unclear why robust loss functions can underfit. We show that most loss functions can be rewritten into a form with the same class-score margin and different sample-weighting functions. The resulting curriculum view provides a straightforward analysis of the training dynamics, which helps attribute underfitting to diminished average sample weights and noise robustness to larger weights for clean samples. We show that simple fixes to the curriculums can make underfitting robust loss functions competitive with the state-of-the-art, and training schedules can substantially affect the noise robustness even with robust loss functions. Code is available at [github](#).

## 1 INTRODUCTION

Label noise is non-negligible in automatic annotation (Liu et al., 2021), crowd-sourcing (Rusakovskiy et al., 2015) and expert annotation (Kato & Matsubara, 2010). Their adverse impacts can be mitigated with loss functions that are theoretically robust against label noise (Song et al., 2020), whose robustness is supported by bounding the difference between expected risk minimizers obtained with clean or noisy labels (Ghosh et al., 2017; Zhou et al., 2021b). However, these bounds do not consider how minimizers are approached or whether they apply to empirically obtained local optimums, leaving open questions on the empirical performance. For example, robust loss functions can underfit (Zhang & Sabuncu, 2018; Wang et al., 2019c) difficult tasks, but the underlying reason cannot be derived from these bounds.

To address such limitations, we analyze training dynamics towards the risk minimizers to characterize the empirical performance of different loss functions. We rewrite loss functions into a form with equivalent gradients, which consists of *the same* class-score margin and *different* sample-weighting functions. The former is a lower bound of the score difference between the labeled class and any other classes, which determines the *direction* of the sample gradient. The latter *weight* samples based on their class-score margins. Interactions between distributions of class-score margins and sample weighting functions thus reveal aspects of the training dynamics. Notably, loss functions with our derived form *implicitly* define different *sample-weighting curriculums* (§4). Here a curriculum, by definition (Wang et al., 2020), specifies a sequence of re-weighting for the distribution of training samples, e.g., sample weighting (Chang et al., 2017) or sample selection (Zhou et al., 2021a), based on a metric for sample difficulty.

We first attribute the underfitting issue to diminished average sample weights during training (§5.1). In particular, classification with more classes lead to smaller class-score margins at initialization, which can lead to minimal sample weights given some robust loss functions. Robust loss functions that severely underfit can become competitive with the best-performing ones by adapting the sample-weighting functions to the number of classes. We then attribute the noise robustness of loss functions to larger weights for clean samples than noise samples (§5.2). We find that dynamics of SGD suppress the learning of noise samples or even get them unlearned. The sample-weighting functions of robust loss functions then magnify differences in the learning pace between clean and noise samples and neglect the unlearned noise samples. Finally, to support our understanding of the training dynamics, we present surprising results that deviate from existing theoretical bounds:

\*Work mainly done at Westlake University.

by simply modifying the learning rate schedule, (1) robust loss functions can become vulnerable to label noise, and (2) cross entropy can appear robust.

## 2 RELATED WORK

Most existing studies on robust loss functions (Ghosh et al., 2017; Zhang & Sabuncu, 2018; Wang et al., 2019c; Feng et al., 2020; Liu & Guo, 2020; Cheng et al., 2021; Zhou et al., 2021b) focus on deriving bounds of the difference between risk minimizers obtained with noisy and clean labels, which are agnostic to the training dynamics. We instead analyze the training dynamics of robust loss functions for reasons behind their underfitting and noise robustness. Although the underfitting issue has been heuristically mitigated with loss combination (Zhang & Sabuncu, 2018; Wang et al., 2019c; Ma et al., 2020), we aim to explicitly identify the cause and support it with our fixes.

Our curriculum view connects existing robust loss functions to the seemingly distinct (Song et al., 2020) curriculum learning. To mitigate the adverse impacts of noisy labels, curriculum-based approaches use either sample selection (Chen et al., 2019; Huang et al., 2019; Zhou et al., 2021a) or sample weighting (Chang et al., 2017; Ren et al., 2018; Wang et al., 2019a;b). Our work is related to studies of sample-weighting curriculums but differs in four perspectives. First, the sample weights analyzed in our work are *implicitly* defined by robust loss functions rather than *explicitly* designed (Chang et al., 2017; Wang et al., 2019a;b) or predicted by a model (Jiang et al., 2018; Ren et al., 2018). Second, the sample difficulty metric of the implicit sample-weighting curriculums is the class-score margin we derived rather than common ones based on loss values (Kumar et al., 2010; Loshchilov & Hutter, 2015) or gradient magnitudes (Gopal, 2016). Third, instead of designing better sample-weighting curriculums (Chang et al., 2017; Wang et al., 2019a;b), we focus on characterizing the performance of *existing* robust loss functions by analyzing their implicit sample-weighting curriculums. Finally, although existing work (Jiang et al., 2018) provides a robust-loss-function view of some sample-weighting curriculums by identifying their effective loss functions, we focus on the curriculum view of *existing* robust loss functions.

Our work is also related to the ongoing debate (Hacohen & Weinshall, 2019; Wang et al., 2020) on the strategies to select or weight samples in curriculum learning: either easier first (Bengio et al., 2009; Kumar et al., 2010) or harder first (Loshchilov & Hutter, 2015; Zhang et al., 2018). In contrast, the sample-weighting functions we identified in robust loss functions can be viewed as a combination of both strategies, emphasizing samples with moderate difficulty.

## 3 BACKGROUND

We formulate classification with label noise and noise robustness and briefly review existing research on robust loss functions before diving into our curriculum view.

**Classification**  $k$ -ary classification with input  $\mathbf{x} \in \mathbb{R}^d$  can be solved with classifier  $\arg \max_i s_i$ , where  $s_i$  is the score of the  $i$ -th class in scoring function  $\mathbf{s}_\theta : \mathbb{R}^d \rightarrow \mathbb{R}^k$  parameterized by  $\theta$ .  $s_i$  can be converted into probability  $p_i$  with the softmax function  $p_i = e^{s_i} / \sum_j e^{s_j}$ . Given the ground truth label  $y^* \in \{1..k\}$  for  $\mathbf{x}$  and a loss function  $L(\mathbf{s}_\theta(\mathbf{x}), y^*)$ , we can estimate  $\theta$  with risk minimization  $\arg \min_\theta \mathbb{E}_{\mathbf{x}, y^*} [L(\mathbf{s}_\theta(\mathbf{x}), y^*)]$ .

**Noise robustness** Labeling errors can corrupt the ground truth label  $y^*$  into a noisy one,

$$y = \begin{cases} y^*, & \text{with probability } P(y = y^* | \mathbf{x}, y^*) \\ i, i \neq y^* & \text{with probability } P(y = i | \mathbf{x}, y^*) \end{cases}$$

Samples  $(\mathbf{x}, y)$  with noisy label  $y$  are clean samples if  $y = y^*$  and noise samples otherwise. Following Ghosh et al. (2017), label noise is *symmetric* (or uniform) if  $P(\tilde{y} = i | \mathbf{x}, y) = \eta / (k - 1), \forall i \neq y$  and *asymmetric* (or class-conditional) when  $P(\tilde{y} = i | \mathbf{x}, y) = P(\tilde{y} = i | y)$ , where  $\eta = P(\tilde{y} \neq y)$  is the noise rate. Given a noisy label  $\tilde{y}$  for  $\mathbf{x}$ , a loss function  $L$  is robust against label noise if

$$\arg \min_\theta \mathbb{E}_{\mathbf{x}, \tilde{y}} L(\mathbf{s}_\theta(\mathbf{x}), \tilde{y}) \approx \arg \min_\theta \mathbb{E}_{\mathbf{x}, y} L(\mathbf{s}_\theta(\mathbf{x}), y)$$

approximately holds. We rewrite  $\mathbf{s}_\theta(\mathbf{x})$  into  $\mathbf{s}$  for notation simplicity hereafter.

### 3.1 TYPICAL ROBUST LOSS FUNCTIONS

We briefly review typical robust loss functions besides cross entropy (CE) that is vulnerable (Ghosh et al., 2017) to label noise. See Table 1 for the formulae and Appendix A for the derivations and extra loss functions.

**Symmetric** A loss function  $L$  is *symmetric* (Ghosh et al., 2017) if

$$\sum_{i=1}^k L(\mathbf{s}, i) = C, \forall \mathbf{s} \in \mathbb{R}^k,$$

with a constant  $C$ . It is robust against *symmetric* label noise when  $\eta < (k-1)/k$ . Mean absolute error (MAE; Ghosh et al., 2017) and the equivalent reverse cross entropy (RCE; Wang et al., 2019c) are both symmetric. Ma et al. (2020) make loss functions with  $L(\mathbf{s}, i) > 0, \forall i \in \{1..k\}$  symmetric by normalizing them,  $L'(\mathbf{s}, y) = L(\mathbf{s}, y) / \sum_i L(\mathbf{s}, i)$ . We include normalized cross entropy (NCE; Ma et al. 2020) as an example.

**Asymmetric**  $L$  as a function of the softmax probability  $p_i$ ,  $L(\mathbf{s}, i) = l(p_i)$ , is *asymmetric* (Zhou et al., 2021b) if

$$\tilde{r} = \max_{i \neq y} \frac{P(\tilde{y} = i | \mathbf{x}, y)}{P(\tilde{y} = y | \mathbf{x}, y)} \leq \inf_{\substack{0 \leq p_i, p_j \leq 1 \\ p_i + p_j \leq 1}} \frac{l(p_i) - l(p_i + p_j)}{l(0) - l(p_j)},$$

where  $p_j$  is a valid increment of  $p_i$ . An asymmetric loss function is robust against *generic* label noise when  $\tilde{r} < 1$ , i.e., there are more clean samples than noisy samples. We include asymmetric generalized cross entropy (AGCE) and asymmetric unhinged loss (AUL) from Zhou et al. (2021b).

**Combined** Robust loss functions that underfit (Zhang & Sabuncu, 2018) can be combined with loss functions like CE to balance robustness and sufficient learning. For example, generalized cross entropy (GCE; Zhang & Sabuncu, 2018) is a smooth interpolation between CE and MAE. Alternatively, symmetric cross entropy (SCE; Wang et al., 2019c) is a weighted average of CE and RCE (MAE). Ma et al. (2020) propose to combine active and passive loss functions with weighted average. We include NCE+MAE as an example.

### 3.2 EXPLAINING UNDERFITTING OF ROBUST LOSS FUNCTIONS

Despite the theoretical bounds for noise robustness, robust loss functions such as MAE can underfit difficult tasks (Zhang & Sabuncu, 2018). Existing explanations can be limited. Zhang & Sabuncu (2018) attribute underfitting of MAE to the lack of the  $1/p_y$  term in the sample gradient compared to CE, thus “treating every sample equally” and hampering learning. However, we show that MAE instead emphasizes samples with moderate class-score margins after factoring sample gradients into weights and directions. Ma et al. (2020) attribute underfitting to failure in balancing the active-passive components. They rewrite loss functions into  $L(\mathbf{s}, y) = \sum_i l(\mathbf{s}, i)$  where  $i \in \{1..k\}$  is an arbitrary class, and define active loss functions with  $\forall i \neq y, l(\mathbf{s}, i) = 0$ , which emphasizes learning the labeled class  $y$ . In contrast, passive loss functions defined with  $\exists i \neq y, l(\mathbf{s}, i) \neq 0$  can be improved by unlearning other classes  $i \neq y$ . However, since there is no canonical guideline to specify  $l(\mathbf{s}, i)$ , different specifications can lead to ambiguities. Given

$$L_{\text{MAE}}(\mathbf{s}, y) \propto \sum_i |\mathbb{I}(i = y) - p_i| \propto \sum_i \mathbb{I}(i = y)(1 - p_i)$$

with indicator function  $\mathbb{I}(\cdot)$ , MAE is active if  $l(\mathbf{s}, i) = \mathbb{I}(i = y)(1 - p_i)$  but passive if  $l(\mathbf{s}, i) = |\mathbb{I}(i = y) - p_i|$ . Finally, Wang et al. (2019a) view  $\|\nabla_{\mathbf{s}} L(\mathbf{s}, y)\|_1$  as weights for sample gradients and attribute underfitting to their low variance, making clean and noise samples less distinguishable. However, as shown in §5.1, MAE also underfits data with clean labels. We provide an alternative explanation with our curriculum view in §5.1, which leads to effective fixes for the issue.

## 4 IMPLICIT CURRICULUMS OF LOSS FUNCTIONS

We derive the main results of our curriculum view for later analysis. The softmax probability  $p_y$  of the (noisily) labeled class  $y$  can be written into a sigmoid form,

$$p_y = \frac{e^{s_y}}{\sum_i e^{s_i}} = \frac{1}{e^{-(s_y - \log \sum_{i \neq y} e^{s_i})} + 1} = \frac{1}{e^{-\Delta_y} + 1},$$

Type	Name	Function	Sample Weight $w$	Constraints
/	CE	$-\log p_y$	$1 - p_y$	/
Sym.	MAE/RCE	$1 - p_y$	$p_y(1 - p_y)$	/
	NCE	$-\log p_y / \left(\sum_{i=1}^k -\log p_i\right)$	/	/
Asym.	AUL	$[(a - p_y)^q - (a - 1)^q]/q$	$p_y(1 - p_y)(a - p_y)^{q-1}$	$a > 1, q > 0$
	AGCE	$[(a + 1) - (a + p_y)^q]/q$	$p_y(a + p_y)^{q-1}(1 - p_y)$	$a > 0, q > 0$
Comb.	GCE	$(1 - p_y^q)/q$	$p_y^q(1 - p_y)$	$0 < q \leq 1$
	SCE	$(1 - q) \cdot L_{\text{CE}} + q \cdot L_{\text{MAE}}$	$(1 - q + q \cdot p_y)(1 - p_y)$	$0 < q < 1$
	NCE+MAE	$(1 - q) \cdot L_{\text{NCE}} + q \cdot L_{\text{MAE}}$	/	$0 < q < 1$

Table 1: Expressions, constraints and sample-weighting functions (§4) for loss functions in §3.1.

where

$$\Delta_y = s_y - \log \sum_{i \neq y} e^{s_i} \leq s_y - \max_{i \neq y} s_i$$

is the soft score margin between the labeled class  $y$  and any other classes. A large  $\Delta_y$  indicates a well-learned sample as  $\Delta_y \geq 0$  leads to successful classification with  $y = \arg \max_i s_i$ . Note that loss functions in Table 1 except NCE and NCE+MAE are functions of  $p_y$ ,  $L(\mathbf{s}, y) = l(p_y)$ . Given

$$\nabla_{\mathbf{s}} L(\mathbf{s}, y) = \nabla_{\mathbf{s}} l(p_y) = \frac{dl}{dp_y} \frac{dp_y}{d\Delta_y} \cdot \nabla_{\mathbf{s}} \Delta_y = \nabla_{\mathbf{s}} \left[ \rho \left( \frac{dl}{dp_y} \frac{dp_y}{d\Delta_y} \right) \cdot \Delta_y \right] = \nabla_{\mathbf{s}} [w(\Delta_y) \cdot \Delta_y],$$

where  $\rho(\cdot)$  is the stop-gradient operator, we can rewrite  $L$  into a form with equivalent gradient,

$$\tilde{L}(\mathbf{s}, y) = w(\Delta_y) \cdot \Delta_y, \quad (1)$$

where  $w(\Delta_y) = \rho\left(\frac{dl}{dp_y} \frac{dp_y}{d\Delta_y}\right) \leq 0$  is the *sample-weighting function*. A larger  $|w(\Delta_y)|$  emphasizes more on increasing  $\Delta_y$  of the sample. Since  $\|\nabla_{\mathbf{s}} \Delta_y\|_1 = 2$ ,  $\Delta_y$  determines the direction of sample gradients. Thus Eq. (1) essentially factorizes the weight and direction of sample gradients. Loss functions in the form of Eq. (1) differ only in the sample-weighting functions  $w(\Delta_y)$ , each implicitly defines a *sample-weighting curriculum* based on  $\Delta_y$  that reflects sample difficulty. Compared to existing sample-difficulty metrics like loss value (Kumar et al., 2010) or gradient magnitude (Gopal, 2016),  $\Delta_y$  factors out the nonlinear preference of  $w(\Delta_y)$  and can be a better drop-in replacement in curriculum-based approaches. The interactions between  $w(\Delta_y)$  and distributions of  $\Delta_y$  further reveal training dynamics with different loss functions, which facilitate our analysis in §5. See Table 1 for  $w(\Delta_y)$  of the reviewed loss functions, and Appendix A for how hyperparameters affect  $w(\Delta_y)$ .

#### 4.1 THE ADDITIONAL REGULARIZER OF NCE

NCE does not exactly follow Eq. (1) as it additionally depends on  $p_i$  with class  $i \neq y$ . However, with equivalent gradients, it can be rewritten into

$$\tilde{L}_{\text{NCE}}(\mathbf{s}, y) = \gamma \cdot L_{\text{CE}}(\mathbf{s}, y) + \gamma \cdot \epsilon \cdot R_{\text{NCE}}(\mathbf{s}), \quad (2)$$

with  $\gamma = \rho(-1/\sum_i \log p_i)$  and  $\epsilon = \rho(k \log p_y / \sum_i \log p_i)$  the weights and  $\rho(\cdot)$  the stop-gradient operator. Both  $\gamma$  and  $\epsilon$  decrease as  $\Delta_y$  increases. The first additive term in Eq. (2) is a *primary loss function* following Eq. (1), which defines a sample-weighting curriculum. The second is a *regularizer*

$$R_{\text{NCE}}(\mathbf{s}) = \sum_{i=1}^k \frac{1}{k} \log p_i$$

that reduces the entropy of softmax outputs and decreases  $\gamma$  and  $\epsilon$ . Although training dynamics of NCE are complicated by the extra regularizer, the L1 norm of sample gradients can be bounded with

$$\|\nabla_{\mathbf{s}} L_{\text{NCE}}(\mathbf{s}, y)\|_1 \leq 2\gamma \cdot (1 + \epsilon) \cdot w_{\text{CE}} \quad (3)$$

Loss	CIFAR10			CIFAR100		
	Train	Test	$\alpha_t$	Train	Test	$\alpha_t$
CE	99.98	92.96	45.74	99.97	71.02	86.79
SCE	99.99	93.20	19.72	99.97	71.11	30.63
GCE	99.97	92.78	23.72	99.90	70.14	30.86
NCE+MAE	99.68	92.35	/	92.30	68.28	/
AUL	99.93	91.80	4.49	88.19	59.62	2.11
AGCE	99.83	92.88	17.20	66.99	51.33	9.24
NCE	99.92	91.17	/	31.64	29.67	/
MAE	98.67	91.93	4.05	10.32	9.85	0.28
AUL <sup>†</sup>	98.80	92.06	3.25	9.22	8.67	0.21
AGCE <sup>†</sup>	91.60	86.30	3.98	3.82	3.82	0.12

Table 2: With clean labels, robust loss functions can underfit CIFAR100 but CIFAR10. We report the average accuracies and  $\alpha_t$  (scaled by  $10^4$ ) at the final training step with learning rate  $\eta = 0.1$  from 3 different runs. See Appendix C.1 for hyperparameters of loss functions tuned on CIFAR100 in Table 8. Settings with inferior hyperparameters are denoted with  $\dagger$ .

which helps explain why NCE can underfit in §5.1. See Appendix A.5 for discussions on similar loss functions with an additional regularizer and detailed derivations.

## 5 LOSS FUNCTIONS WITH THE CURRICULUM VIEW

We examine the interaction between  $w(\Delta_y)$  and  $\Delta_y$  distributions to address questions in §3.2. Results are reported on MNIST (Lecun et al., 1998) and CIFAR10/100 (Krizhevsky, 2009) with synthetic symmetric and asymmetric label noise following Ma et al. (2020); Zhou et al. (2021b). For real-world scenarios, we include CIFAR10/100 with human label noise (Wei et al., 2022) and the large-scale noisy dataset WebVision (Li et al., 2017), which exhibit more complex noise patterns than symmetric and asymmetric label noise. Unlike standard settings, we scale  $w(\Delta_y)$  to unit maximum to avoid complications, since hyperparameters of loss functions can change the scale of  $w(\Delta_y)$ , essentially adjusting the learning rate of SGD. See Appendix B for more experimental details.

### 5.1 UNDERSTANDING UNDERFITTING OF ROBUST LOSS FUNCTIONS

We reproduce the underfitting issue without label noise in Table 2. The hyperparameters of loss functions are tuned on CIFAR100 and listed in Table 8 of Appendix C.1. CE outperforms NCE, AGCE, AUL and MAE by a nontrivial margin on CIFAR100. The less performant loss functions has smaller gap between training and testing performance, suggesting the issue of underfitting. In contrast, all loss functions performs equally well on CIFAR10.

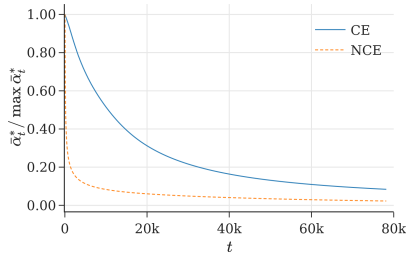
**Marginal sample weights explains underfitting.** Since the same model fits each dataset well with CE in Table 2, underfitting should result from insufficient parameter updates with the altered loss functions rather than inadequate model size. Based on our derivation, the average scale of parameter update up to  $t$ -th step can be estimated with

$$\alpha_t = \frac{\sum_{i=1}^t \sum_{s \in \mathcal{B}_i} \eta_i \cdot \|\nabla_s \Delta_y\|_1}{\sum_{i=1}^t \eta_i \cdot |\mathcal{B}_i|}$$

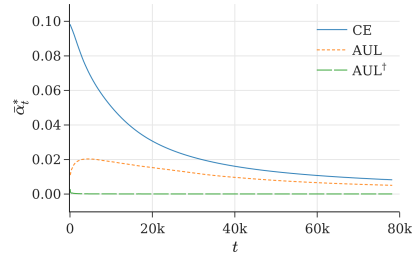
where  $\eta_i$  is the learning rate and  $\mathcal{B}_i$  the sampled batch at training step  $i$ . As shown in Table 2, at the final training step, a small  $\alpha_t$  highly correlates with underfitting.

**Fast diminishing sample weights lead to underfitting.** In Fig. 1a,  $\alpha_t$  of NCE peaks at initialization similar to CE. However, it decreases much faster than CE since both  $\gamma$  and  $\epsilon$  decrease with improved  $\Delta_y$ . The regularizer  $R_{\text{NCE}}(s)$  further reduces the entropy of softmax output and thus  $\gamma$ . As a result, the fast decreasing  $\alpha_t$  hampers the learning of training samples and leads to underfitting.

**Marginal initial sample weights lead to underfitting.** Unlike NCE, loss functions that severely underfit in Table 2 assign marginal initial weights (Fig. 2c) to samples in CIFAR100, which leads to marginal initial  $\alpha_t$ .  $\Delta_y$  of these samples can barely improve before the learning rate vanishes, thus leading to underfitting. In contrast, loss functions with non-trivial initial sample weights (Fig. 2a and 2b) result in moderate or no underfitting. As further corroboration, we plot  $\alpha_t$  of AUL with

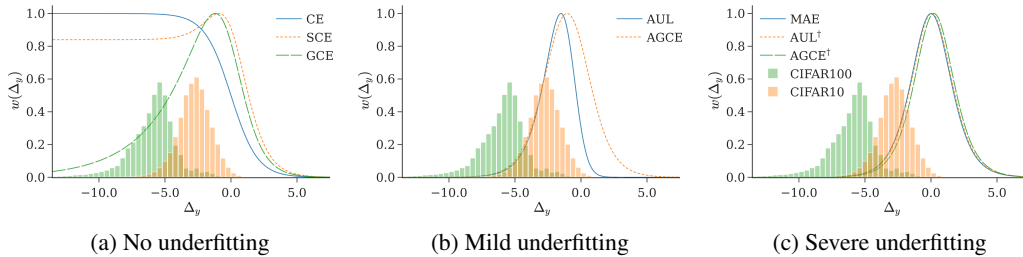


(a) NCE with estimated weight upperbound.



(b) AUL with inferior/superior hyperparameters.

Figure 1: Different explanations for underfitting: (a) fast diminishing sample weights; (b) marginal initial sample weights. We plot the variation of  $\alpha_t$  with training step  $t$  on CIFAR100 without label noise for each loss function.  $\alpha_t$  in (a) is normalized with its maximum to emphasize its variation during training.



(a) No underfitting

(b) Mild underfitting

(c) Severe underfitting

Figure 2: Sample-weighting functions  $w(\Delta_y)$  of loss functions in Table 2 with hyperparameters in Table 8. We include the initial  $\Delta_y$  distributions of training samples on CIFAR10 and CIFAR100 for reference, which are extracted with a randomly initialized model.

superior and inferior hyperparameters (AUL and AUL<sup>†</sup> in Table 2) in Fig. 1b.  $\alpha_t$  stays marginal with AUL<sup>†</sup>, but quickly increases to a non-negligible value before gradually decreasing with AUL.

**Loss combination can mitigate underfitting.** As  $\alpha_t$  of NCE peaks at initialization but quickly diminishes while  $\alpha_t$  of MAE is marginal at initialization but peaks later during training, combining NCE with MAE can mitigate the underfitting issue of each other. In Table 2, combining NCE and MAE suffers less from underfitting compared to both individuals.

**Increased number of classes leads to marginal initial sample weights.** Unlike CIFAR100, loss functions in Table 2 perform equally well on CIFAR10. The difference has been vaguely attributed to the increased task difficulty of CIFAR100 (Zhang & Sabuncu, 2018; Song et al., 2020). Intuitively, the more classes, the more subtle differences to be distinguished. In addition, the number of classes  $k$  determines the initial distribution of  $\Delta_y$ . Assume that class scores  $s_i$  at *initialization* are i.i.d. normal variables  $s_i \sim \mathcal{N}(\mu, \sigma)$ . In particular,  $\mu = 0$  and  $\sigma = 1$  for most neural networks with standard initializations (Glorot & Bengio, 2010; He et al., 2015) and normalization layers (Ioffe & Szegedy, 2015; Ba et al., 2016). The expected  $\Delta_y$  can be approximated with

$$\mathbb{E}[\Delta_y] \approx -\log(k-1) - \sigma^2/2 + \frac{e^{\sigma^2} - 1}{2(k-1)} \quad (4)$$

We leave derivations and comparisons between our assumptions and real settings to Appendix C.1. A large  $k$  results in small initial  $\Delta_y$ ; with sample-weighting functions in Fig. 2c it further leads to marginal initial sample weights, which results in underfitting on CIFAR100 as discussed above.

### 5.1.1 ADDRESSING UNDERFITTING FROM MARGINAL INITIAL SAMPLE WEIGHTS

Our analysis suggests that the fixed sample-weighting function  $w(\Delta_y)$  is to blame for underfitting. Assuming  $\mathbb{E}[\Delta_y] < 0$  at initialization, to address underfitting from marginal initial sample weights, we can simply scale

$$w^*(\Delta_y) = w(\Delta_y^*) = w(\Delta_y / |\mathbb{E}[\Delta_y]| \cdot \tau)$$

or shift

$$w^+(\Delta_y) = w(\Delta_y^+) = w(\Delta_y + |\mathbb{E}[\Delta_y]| - \tau)$$

Loss	Clean	Symmetric		Asymmetric	Human
	$\eta = 0$	$\eta = 0.4$	$\eta = 0.8$	$\eta = 0.4$	$\eta = 0.4$
CE <sup>‡</sup>	71.33 $\pm$ 0.43	39.92 $\pm$ 0.10	7.59 $\pm$ 0.20	40.17 $\pm$ 1.31	/
GCE <sup>‡</sup>	63.09 $\pm$ 1.39	56.11 $\pm$ 1.35	17.42 $\pm$ 0.06	40.91 $\pm$ 0.57	/
NCE <sup>‡</sup>	29.96 $\pm$ 0.73	19.54 $\pm$ 0.52	8.55 $\pm$ 0.37	20.64 $\pm$ 0.40	/
NCE+AUL <sup>‡</sup>	68.96 $\pm$ 0.16	59.25 $\pm$ 0.23	23.03 $\pm$ 0.64	38.59 $\pm$ 0.48	/
AGCE	49.27 $\pm$ 1.03	47.76 $\pm$ 1.75	16.03 $\pm$ 0.59	33.40 $\pm$ 1.57	30.45 $\pm$ 1.50
AGCE shift	69.39 $\pm$ 0.84	48.21 $\pm$ 1.06	14.49 $\pm$ 0.17	40.76 $\pm$ 0.74	48.71 $\pm$ 0.45
AGCE scale	70.57 $\pm$ 0.62	56.69 $\pm$ 0.33	14.64 $\pm$ 0.79	39.71 $\pm$ 0.17	50.85 $\pm$ 0.11
MAE	3.69 $\pm$ 0.59	1.29 $\pm$ 0.50	1.00 $\pm$ 0.00	2.53 $\pm$ 1.34	2.09 $\pm$ 0.55
MAE shift	68.57 $\pm$ 0.54	49.95 $\pm$ 0.16	13.10 $\pm$ 0.41	39.83 $\pm$ 0.18	47.91 $\pm$ 0.36
MAE scale	<b>70.97 <math>\pm</math> 0.41</b>	<b>60.57 <math>\pm</math> 1.04</b>	<b>24.44 <math>\pm</math> 0.73</b>	<b>44.48 <math>\pm</math> 1.05</b>	<b>54.70 <math>\pm</math> 0.48</b>

Table 3: Shifting or scaling  $w(\Delta_y)$  mitigates underfitting on CIFAR100 under different label noise. We report test accuracies with 3 different runs. Results from Zhou et al. (2021b) are included as context (denoted with ‡). See Appendix C.1 for hyperparameter  $\tau$  and results with more noise rates.

Settings	$k = 50$	$k = 200$	$k = 400$
	$\tau = 2.0$	$\tau = 1.8$	$\tau = 1.6$
CE	66.40	70.26	70.16
MAE	3.68	0.50	0.25
MAE shift	60.76	59.31	47.32
MAE scale	<b>66.72</b>	<b>71.92</b>	<b>71.87</b>

Table 4: Shifting or scaling  $w(\Delta_y)$  mitigates underfitting on WebVision subsampled with different numbers of classes.  $k = 50$  is the standard “mini” setting in previous work (Ma et al., 2020; Zhou et al., 2021b). We report test accuracy with a single run due to a limited computation budget.

the sample-weighting functions, where  $\tau$  is a hyperparameter. Intuitively, both approaches cancel the effect of large  $k$  on the weight of  $\mathbb{E}[\Delta_y]$  at initialization. A small  $\tau$  thus leads to high initial sample weights regardless of  $k$ . See Appendix C.1.1 for visualizations of the scaled and shifted sample-weighting functions and discussions on the robustness of loss functions they induce.

We report results on CIFAR100 with different label noise in Table 3, and results on the noisy large-scale dataset WebVision in Table 4. In summary, shifting and scaling alleviate underfitting, making MAE and AGCE comparable to the previous state-of-the-art (NCE+AUL; Zhou et al. 2021b). Notably,  $w^*(\Delta_y)$  leads to dramatic improvements for MAE under all settings. Interestingly, although  $w^*(\Delta_y)$  and  $w^+(\Delta_y)$  are both agnostic to the number of classes at initialization, their performances differ significantly. Intuitively,  $w^+(\Delta_y)$  diminishes much faster than  $w^*(\Delta_y)$  with increased  $\Delta_y$ , which can lead to insufficient training of clean samples and thus inferior performance.

## 5.2 UNDERSTANDING NOISE ROBUSTNESS OF LOSS FUNCTIONS

We show that robust loss functions following Eq. (1) *implicitly* assign larger weights to clean samples. The underlying reasons are explored by examining how  $\Delta_y$  distributions change during training. Notably, similar sample-weighting rules are *explicitly* adopted by curriculums for noise robust training (Ren et al., 2018). We leave NCE to future work as it involves an additional regularizer.

**Robust loss functions assign larger weights to clean samples.** We use the ratio between the average weights of clean ( $\bar{w}_{\text{clean}}$ ) and noisy ( $\bar{w}_{\text{noise}}$ ) samples,  $\text{snr} = \bar{w}_{\text{clean}}/\bar{w}_{\text{noise}}$ , to characterize their relative contribution during training. See Appendix C.2 for the exact formulas. Noise robustness is characterized by differences in test accuracy compared to results with clean labels (diff). We report diff and snr under different label noise on CIFAR10 in Table 5. Loss functions with higher snr have less performance drop with label noise in general, thus being more robust.

To explain what leads to a large snr, we plot changes of  $\Delta_y$  distributions during training on CIFAR10 with symmetric label noise in Fig. 3. When trained with loss functions that are more robust against label noise (Fig. 3b and 3c),  $\Delta_y$  distributions of noisy and clean samples spread wider and get better separated. In addition, the consistent decrease of  $\Delta_y$  for noisy samples suggests that they can be *unlearned*. In contrast, training with CE (Fig. 3a) results in more compact and less separated  $\Delta_y$  distributions. Furthermore,  $\Delta_y$  of noisy samples consistently increases.

Loss	Clean	Asymmetric		Symmetric				Human			
	Acc	$\eta = 0.2$ diff	snr	$\eta = 0.2$ diff	snr	$\eta = 0.4$ diff	snr	$\eta = 0.8$ diff	snr	$\eta = 0.4$ diff	snr
CE	90.64	-7.06	0.32	-15.47	0.39	-31.95	0.57	-50.87	0.77	-28.51	0.53
SCE	89.87	-5.39	0.51	-3.84	0.99	-10.47	1.27	-27.25	1.51	-15.84	0.86
GCE	90.44	-7.42	0.36	-6.80	0.96	-23.23	0.89	-45.32	1.04	-21.94	0.72
AUL	89.90	-2.51	0.81	-2.07	3.10	-5.87	2.96	-13.90	2.83	-12.08	1.11
MAE	89.29	-2.21	1.00	-1.92	3.56	-4.36	3.33	-11.53	3.22	-10.35	1.32
AGCE	82.62	-9.42	0.92	-1.55	3.02	-19.90	2.16	-41.11	1.83	-21.73	1.28

Table 5: Robust loss functions assign larger weights to clean samples. We report snr and diff from the best of 5 runs on CIFAR10 under each noise setting, as inferior initialization can heavily degrade the performance. Hyperparameters listed in Table 12 are selected to cover more variants of sample-weighting functions (plotted in Fig. 8), which are not necessarily optimal.

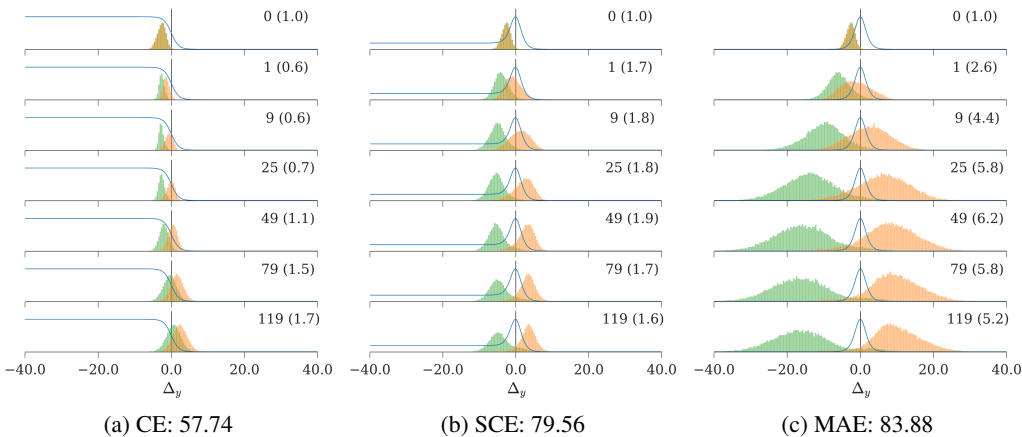


Figure 3: How  $\Delta_y$  distributions of noisy (green, left) and clean (orange, right) samples change on CIFAR10 during training with symmetric label noise and  $\eta = 0.4$ . Vertical axes denoting probability density are scaled to the peak of histograms for readability, with epoch number (axis scaling factor) denoted on the right of each subplot. We plot  $w(\Delta_y)$  and report the test accuracy of each setting for reference. See Appendix C.2 for results with additional types of label noise and loss functions.

**Dynamics of SGD suppress learning of noisy samples.** As shown in Fig. 3a, noisy samples are learned slower than clean samples as measured by improvements of  $\Delta_y$ , which can be explained by more coherent gradients among clean samples (Chatterjee & Zielinski, 2022). Similar results have been reported (Zhang et al., 2017; Arpit et al., 2017) and utilized in curriculum-based robust training (Yao et al., 2019; Han et al., 2018). In addition, noisy samples can be unlearned as shown in Fig. 3b and 3c, which can stem from generalization with clean samples. Both dynamics suppress the learning of noisy samples but clean ones, thus leading to robustness against label noise.

**Robust  $w(\Delta_y)$  synergizes with SGD dynamics for noise robustness.** In Fig. 2, the bell-shaped  $w(\Delta_y)$  of robust loss functions only assigns large weights to samples with moderate  $\Delta_y$ . Since  $\Delta_y$  distributions initially concentrate at the monotonically increasing interval of  $w(\Delta_y)$ , (1) samples with faster improving  $\Delta_y$ , due to either larger initial weights or faster learning as clean samples, are weighted more during early training and learned faster. The magnified learning pace difference explains the widely spread distributions in Fig. 3b and 3c. In addition, (2) the unlearned samples with small  $\Delta_y$  receive diminishing weights from  $w(\Delta_y)$ , which hampers their pace of learning. Noisy samples in Fig. 3b and 3c are consistently unlearned and ignored with marginal sample weights, leading to a consistent decrease in  $\Delta_y$ . In addition to the SGD dynamics, (1) and (2) further suppress the learning of noisy samples and enhance that of clean samples, thus leading to increased robustness against label noise. In contrast, the monotonically decreasing  $w_{\text{CE}}(\Delta_y)$  emphasizes samples with smaller  $\Delta_y$ , essentially acting against the SGD dynamics for noise robustness. Thus training with CE results in increased vulnerability to label noise as shown in Table 5.



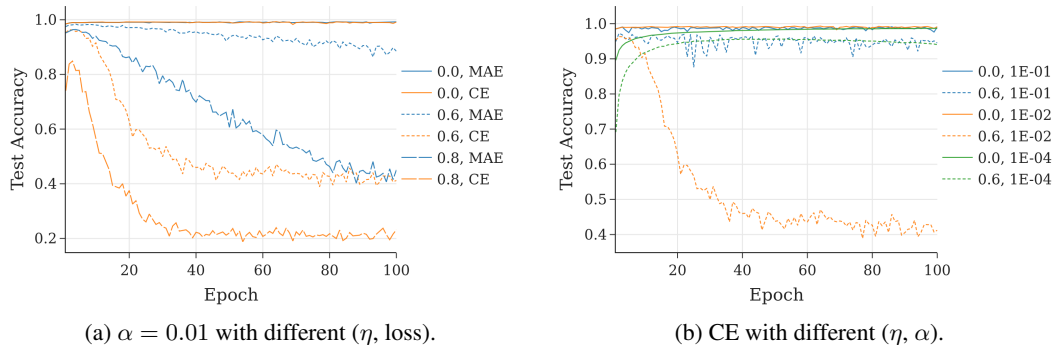


Figure 4: Learning curves with fixed learning rate and extended training epochs on MNIST under symmetric label noise, where  $\alpha$  is the learning rate and  $\eta$  the noise rate.

### 5.2.1 TRAINING SCHEDULES AFFECT NOISE ROBUSTNESS

Although the learning pace of noisy samples gets initially suppressed, the expected gradient will eventually be dominated by noisy samples, since well-learned clean samples receive marginal sample weights thanks to the monotonically decreasing interval of  $w(\Delta_y)$ . Models with extended training<sup>1</sup> thus risk overfitting noisy samples during the late training stage. Adjusting the training schedules to enable or avoid such overfitting can therefore affect the noise robustness of models. Based on this intuition, we present two surprising examples that deviate from existing theoretical results:

**Extended training can make robust loss functions vulnerable to label noise.** The learning curves of CE and MAE with *constant* learning rates on MNIST are shown in Fig. 4a. Despite the theoretically guaranteed noise robustness (Ghosh et al., 2017), similar to CE, with extended training, MAE eventually overfits noisy samples, resulting in vulnerability to label noise.

**CE can become robust by adjusting the learning rate schedule.** To avoid overfitting noisy samples, we can avoid learning when noisy samples dominate the expected gradient. It can be achieved with either early stopping (Song et al., 2019), or a constrained learning pace that prevents sufficient learning of clean samples, which avoids diminishing weights for them. We show the learning curve of CE using fixed learning rates under symmetric label noise on MNIST in Fig. 4b. By simply increasing or decreasing the learning rate, which strengthens the implicit regularization of SGD (Smith et al., 2021) or directly slows down the learning pace, CE can become robust against label noise.

## 6 CONCLUSION AND DISCUSSIONS

We extend the understanding of robust loss functions by considering the training dynamics to reach the risk minimizers. By rewriting numerous loss functions into the same class-score margin and varied sample-weighting functions, we explicitly connect the design of loss functions to the design of sample-weighting curriculums and unify a broad array of loss functions. Based on the curriculum view, we gain more insights into how robust loss functions work and propose effective fixes to address the underfitting issue of robust loss functions.

## REFERENCES

- Devansh Arpit, Stanislaw Jastrzebski, Nicolas Ballas, David Krueger, Emmanuel Bengio, Maxinder S. Kanwal, Tegan Maharaj, Asja Fischer, Aaron C. Courville, Yoshua Bengio, and Simon Lacoste-Julien. A closer look at memorization in deep networks. In Doina Precup and Yee Whye Teh (eds.), *Proceedings of the 34th International Conference on Machine Learning, ICML 2017, Sydney, NSW, Australia, 6-11 August 2017*, volume 70 of *Proceedings of Machine Learning Research*, pp. 233–242. PMLR, 2017. URL <http://proceedings.mlr.press/v70/arpit17a.html>.
- Jimmy Lei Ba, Jamie Ryan Kiros, and Geoffrey E. Hinton. Layer normalization, 2016. URL <https://arxiv.org/abs/1607.06450>.

<sup>1</sup>Enough training steps without early stopping or diminishing learning rates for a small training loss.

- Yoshua Bengio, Jérôme Louradour, Ronan Collobert, and Jason Weston. Curriculum learning. In Andrea Pohoreckyj Danyluk, Léon Bottou, and Michael L. Littman (eds.), *Proceedings of the 26th Annual International Conference on Machine Learning, ICML 2009, Montreal, Quebec, Canada, June 14-18, 2009*, volume 382 of *ACM International Conference Proceeding Series*, pp. 41–48. ACM, 2009. doi: 10.1145/1553374.1553380. URL <https://doi.org/10.1145/1553374.1553380>.
- Haw-Shiuan Chang, Erik G. Learned-Miller, and Andrew McCallum. Active bias: Training more accurate neural networks by emphasizing high variance samples. In Isabelle Guyon, Ulrike von Luxburg, Samy Bengio, Hanna M. Wallach, Rob Fergus, S. V. N. Vishwanathan, and Roman Garnett (eds.), *Advances in Neural Information Processing Systems 30: Annual Conference on Neural Information Processing Systems 2017, December 4-9, 2017, Long Beach, CA, USA*, pp. 1002–1012, 2017. URL <https://proceedings.neurips.cc/paper/2017/hash/2f37d10131f2a483a8dd005b3d14b0d9-Abstract.html>.
- Satrajit Chatterjee and Piotr Zielinski. On the generalization mystery in deep learning. *ArXiv preprint*, abs/2203.10036, 2022. URL <https://arxiv.org/abs/2203.10036>.
- Pengfei Chen, Benben Liao, Guangyong Chen, and Shengyu Zhang. Understanding and utilizing deep neural networks trained with noisy labels. In Kamalika Chaudhuri and Ruslan Salakhutdinov (eds.), *Proceedings of the 36th International Conference on Machine Learning, ICML 2019, 9-15 June 2019, Long Beach, California, USA*, volume 97 of *Proceedings of Machine Learning Research*, pp. 1062–1070. PMLR, 2019. URL <http://proceedings.mlr.press/v97/chen19g.html>.
- Hao Cheng, Zhaowei Zhu, Xingyu Li, Yifei Gong, Xing Sun, and Yang Liu. Learning with instance-dependent label noise: A sample sieve approach. In *9th International Conference on Learning Representations, ICLR 2021, Virtual Event, Austria, May 3-7, 2021*. OpenReview.net, 2021. URL <https://openreview.net/forum?id=2VXyy9mIyU3>.
- Barry Cobb, Rafael Rumí, and Antonio Salmerón. Approximating the distribution of a sum of log-normal random variables. 2012.
- Lei Feng, Senlin Shu, Zhuoyi Lin, Fengmao Lv, Li Li, and Bo An. Can cross entropy loss be robust to label noise? In Christian Bessiere (ed.), *Proceedings of the Twenty-Ninth International Joint Conference on Artificial Intelligence, IJCAI 2020*, pp. 2206–2212. ijcai.org, 2020. doi: 10.24963/ijcai.2020/305. URL <https://doi.org/10.24963/ijcai.2020/305>.
- Aritra Ghosh, Himanshu Kumar, and P. S. Sastry. Robust loss functions under label noise for deep neural networks. In Satinder P. Singh and Shaul Markovitch (eds.), *Proceedings of the Thirty-First AAAI Conference on Artificial Intelligence, February 4-9, 2017, San Francisco, California, USA*, pp. 1919–1925. AAAI Press, 2017. URL <http://aaai.org/ocs/index.php/AAAI/AAAI17/paper/view/14759>.
- Xavier Glorot and Yoshua Bengio. Understanding the difficulty of training deep feedforward neural networks. In *Proceedings of the Thirteenth International Conference on Artificial Intelligence and Statistics*, pp. 249–256. JMLR Workshop and Conference Proceedings, 2010. URL <https://proceedings.mlr.press/v9/glorot10a.html>.
- Siddharth Gopal. Adaptive sampling for SGD by exploiting side information. In Maria-Florina Balcan and Kilian Q. Weinberger (eds.), *Proceedings of the 33rd International Conference on Machine Learning, ICML 2016, New York City, NY, USA, June 19-24, 2016*, volume 48 of *JMLR Workshop and Conference Proceedings*, pp. 364–372. JMLR.org, 2016. URL <http://proceedings.mlr.press/v48/gopal16.html>.
- Guy Hacohen and Daphna Weinshall. On the power of curriculum learning in training deep networks. In Kamalika Chaudhuri and Ruslan Salakhutdinov (eds.), *Proceedings of the 36th International Conference on Machine Learning, ICML 2019, 9-15 June 2019, Long Beach, California, USA*, volume 97 of *Proceedings of Machine Learning Research*, pp. 2535–2544. PMLR, 2019. URL <http://proceedings.mlr.press/v97/hacohen19a.html>.

- Bo Han, Quanming Yao, Xingrui Yu, Gang Niu, Miao Xu, Weihua Hu, Ivor W. Tsang, and Masashi Sugiyama. Co-teaching: Robust training of deep neural networks with extremely noisy labels. In Samy Bengio, Hanna M. Wallach, Hugo Larochelle, Kristen Grauman, Nicolò Cesa-Bianchi, and Roman Garnett (eds.), *Advances in Neural Information Processing Systems 31: Annual Conference on Neural Information Processing Systems 2018, NeurIPS 2018, December 3-8, 2018, Montréal, Canada*, pp. 8536–8546, 2018. URL <https://proceedings.neurips.cc/paper/2018/hash/a19744e268754fb0148b017647355b7b-Abstract.html>.
- Kaiming He, Xiangyu Zhang, Shaoqing Ren, and Jian Sun. Delving deep into rectifiers: Surpassing human-level performance on imagenet classification. In *2015 IEEE International Conference on Computer Vision, ICCV 2015, Santiago, Chile, December 7-13, 2015*, pp. 1026–1034. IEEE Computer Society, 2015. doi: 10.1109/ICCV.2015.123. URL <https://doi.org/10.1109/ICCV.2015.123>.
- Kaiming He, Xiangyu Zhang, Shaoqing Ren, and Jian Sun. Deep residual learning for image recognition. In *2016 IEEE Conference on Computer Vision and Pattern Recognition, CVPR 2016, Las Vegas, NV, USA, June 27-30, 2016*, pp. 770–778. IEEE Computer Society, 2016. doi: 10.1109/CVPR.2016.90. URL <https://doi.org/10.1109/CVPR.2016.90>.
- Jinchi Huang, Lie Qu, Rongfei Jia, and Binqiang Zhao. O2u-net: A simple noisy label detection approach for deep neural networks. In *2019 IEEE/CVF International Conference on Computer Vision, ICCV 2019, Seoul, Korea (South), October 27 - November 2, 2019*, pp. 3325–3333. IEEE, 2019. doi: 10.1109/ICCV.2019.00342. URL <https://doi.org/10.1109/ICCV.2019.00342>.
- Sergey Ioffe and Christian Szegedy. Batch normalization: Accelerating deep network training by reducing internal covariate shift. In Francis R. Bach and David M. Blei (eds.), *Proceedings of the 32nd International Conference on Machine Learning, ICML 2015, Lille, France, 6-11 July 2015*, volume 37 of *JMLR Workshop and Conference Proceedings*, pp. 448–456. JMLR.org, 2015. URL <http://proceedings.mlr.press/v37/ioffe15.html>.
- Lu Jiang, Zhengyuan Zhou, Thomas Leung, Li-Jia Li, and Li Fei-Fei. Mentornet: Learning data-driven curriculum for very deep neural networks on corrupted labels. In Jennifer G. Dy and Andreas Krause (eds.), *Proceedings of the 35th International Conference on Machine Learning, ICML 2018, Stockholmsmässan, Stockholm, Sweden, July 10-15, 2018*, volume 80 of *Proceedings of Machine Learning Research*, pp. 2309–2318. PMLR, 2018. URL <http://proceedings.mlr.press/v80/jiang18c.html>.
- Yoshihide Kato and Shigeki Matsubara. Correcting errors in a treebank based on synchronous tree substitution grammar. In *Proceedings of the ACL 2010 Conference Short Papers*, pp. 74–79, Uppsala, Sweden, 2010. Association for Computational Linguistics. URL <https://aclanthology.org/P10-2014>.
- Alex Krizhevsky. Learning multiple layers of features from tiny images. Technical report, 2009.
- M. Pawan Kumar, Benjamin Packer, and Daphne Koller. Self-paced learning for latent variable models. In John D. Lafferty, Christopher K. I. Williams, John Shawe-Taylor, Richard S. Zemel, and Aron Culotta (eds.), *Advances in Neural Information Processing Systems 23: 24th Annual Conference on Neural Information Processing Systems 2010. Proceedings of a meeting held 6-9 December 2010, Vancouver, British Columbia, Canada*, pp. 1189–1197. Curran Associates, Inc., 2010. URL <https://proceedings.neurips.cc/paper/2010/hash/e57c6b956a6521b28495f2886ca0977a-Abstract.html>.
- Y. Lecun, L. Bottou, Y. Bengio, and P. Haffner. Gradient-based learning applied to document recognition. *Proceedings of the IEEE*, 86(11):2278–2324, 1998. doi: 10.1109/5.726791.
- Wen Li, Limin Wang, Wei Li, Eirikur Agustsson, and Luc Van Gool. Webvision database: Visual learning and understanding from web data, 2017. URL <https://arxiv.org/abs/1708.02862>.
- Tsung-Yi Lin, Priya Goyal, Ross B. Girshick, Kaiming He, and Piotr Dollár. Focal loss for dense object detection. In *IEEE International Conference on Computer Vision, ICCV 2017, Venice*,

- Italy, October 22-29, 2017*, pp. 2999–3007. IEEE Computer Society, 2017. doi: 10.1109/ICCV.2017.324. URL <https://doi.org/10.1109/ICCV.2017.324>.
- Kun Liu, Yao Fu, Chuanqi Tan, Mosha Chen, Ningyu Zhang, Songfang Huang, and Sheng Gao. Noisy-labeled NER with confidence estimation. In *Proceedings of the 2021 Conference of the North American Chapter of the Association for Computational Linguistics: Human Language Technologies*, pp. 3437–3445, Online, 2021. Association for Computational Linguistics. doi: 10.18653/v1/2021.naacl-main.269. URL <https://aclanthology.org/2021.naacl-main.269>.
- Yang Liu and Hongyi Guo. Peer loss functions: Learning from noisy labels without knowing noise rates. In *Proceedings of the 37th International Conference on Machine Learning, ICML 2020, 13-18 July 2020, Virtual Event*, volume 119 of *Proceedings of Machine Learning Research*, pp. 6226–6236. PMLR, 2020. URL <http://proceedings.mlr.press/v119/liu20e.html>.
- Ilya Loshchilov and Frank Hutter. Online batch selection for faster training of neural networks. *ArXiv preprint*, abs/1511.06343, 2015. URL <https://arxiv.org/abs/1511.06343>.
- Michal Lukasik, Srinadh Bhojanapalli, Aditya Krishna Menon, and Sanjiv Kumar. Does label smoothing mitigate label noise? In *Proceedings of the 37th International Conference on Machine Learning, ICML 2020, 13-18 July 2020, Virtual Event*, volume 119 of *Proceedings of Machine Learning Research*, pp. 6448–6458. PMLR, 2020. URL <http://proceedings.mlr.press/v119/lukasik20a.html>.
- Xingjun Ma, Hanxun Huang, Yisen Wang, Simone Romano, Sarah M. Erfani, and James Bailey. Normalized loss functions for deep learning with noisy labels. In *Proceedings of the 37th International Conference on Machine Learning, ICML 2020, 13-18 July 2020, Virtual Event*, volume 119 of *Proceedings of Machine Learning Research*, pp. 6543–6553. PMLR, 2020. URL <http://proceedings.mlr.press/v119/ma20c.html>.
- Giorgio Patrini, Alessandro Rozza, Aditya Krishna Menon, Richard Nock, and Lizhen Qu. Making deep neural networks robust to label noise: A loss correction approach. In *2017 IEEE Conference on Computer Vision and Pattern Recognition, CVPR 2017, Honolulu, HI, USA, July 21-26, 2017*, pp. 2233–2241. IEEE Computer Society, 2017. doi: 10.1109/CVPR.2017.240. URL <https://doi.org/10.1109/CVPR.2017.240>.
- Mengye Ren, Wenyan Zeng, Bin Yang, and Raquel Urtasun. Learning to reweight examples for robust deep learning. In Jennifer G. Dy and Andreas Krause (eds.), *Proceedings of the 35th International Conference on Machine Learning, ICML 2018, Stockholmsmässan, Stockholm, Sweden, July 10-15, 2018*, volume 80 of *Proceedings of Machine Learning Research*, pp. 4331–4340. PMLR, 2018. URL <http://proceedings.mlr.press/v80/ren18a.html>.
- Olga Russakovsky, Jia Deng, Hao Su, Jonathan Krause, Sanjeev Satheesh, Sean Ma, Zhiheng Huang, Andrej Karpathy, Aditya Khosla, Michael Bernstein, Alexander C. Berg, and Li Fei-Fei. Imagenet large scale visual recognition challenge. *arXiv:1409.0575 [cs]*, 2015. URL <http://arxiv.org/abs/1409.0575>. arXiv: 1409.0575.
- Samuel L. Smith, Benoit Dherin, David G. T. Barrett, and Soham De. On the origin of implicit regularization in stochastic gradient descent. In *9th International Conference on Learning Representations, ICLR 2021, Virtual Event, Austria, May 3-7, 2021*. OpenReview.net, 2021. URL [https://openreview.net/forum?id=rq\\_Qr0c1Hyo](https://openreview.net/forum?id=rq_Qr0c1Hyo).
- Hwanjun Song, Minseok Kim, Dongmin Park, and Jae-Gil Lee. How does early stopping help generalization against label noise?, 2019. URL <https://arxiv.org/abs/1911.08059>.
- Hwanjun Song, Minseok Kim, Dongmin Park, Yooju Shin, and Jae-Gil Lee. Learning from noisy labels with deep neural networks: A survey. *ArXiv preprint*, abs/2007.08199, 2020. URL <https://arxiv.org/abs/2007.08199>.
- Christian Szegedy, Vincent Vanhoucke, Sergey Ioffe, Jonathon Shlens, and Zbigniew Wojna. Re-thinking the inception architecture for computer vision. In *2016 IEEE Conference on Computer Vision and Pattern Recognition, CVPR 2016, Las Vegas, NV, USA, June 27-30, 2016*, pp. 2818–2826. IEEE Computer Society, 2016. doi: 10.1109/CVPR.2016.308. URL <https://doi.org/10.1109/CVPR.2016.308>.

- Yee Whye Teh, David Newman, and Max Welling. A collapsed variational bayesian inference algorithm for latent dirichlet allocation. In Bernhard Schölkopf, John C. Platt, and Thomas Hofmann (eds.), *Advances in Neural Information Processing Systems 19, Proceedings of the Twentieth Annual Conference on Neural Information Processing Systems, Vancouver, British Columbia, Canada, December 4-7, 2006*, pp. 1353–1360. MIT Press, 2006. URL <https://proceedings.neurips.cc/paper/2006/hash/532b7cbe070a3579f424988a040752f2-Abstract.html>.
- Xin Wang, Yudong Chen, and Wenwu Zhu. A survey on curriculum learning. *ArXiv preprint*, abs/2010.13166, 2020. URL <https://arxiv.org/abs/2010.13166>.
- Xinshao Wang, Yang Hua, Elyor Kodirov, and Neil M. Robertson. Imae for noise-robust learning: Mean absolute error does not treat examples equally and gradient magnitude’s variance matters. *ArXiv preprint*, abs/1903.12141, 2019a. URL <https://arxiv.org/abs/1903.12141>.
- Xinshao Wang, Elyor Kodirov, Yang Hua, and Neil M. Robertson. Derivative manipulation for general example weighting. *ArXiv preprint*, abs/1905.11233, 2019b. URL <https://arxiv.org/abs/1905.11233>.
- Yisen Wang, Xingjun Ma, Zaiyi Chen, Yuan Luo, Jinfeng Yi, and James Bailey. Symmetric cross entropy for robust learning with noisy labels. In *2019 IEEE/CVF International Conference on Computer Vision, ICCV 2019, Seoul, Korea (South), October 27 - November 2, 2019*, pp. 322–330. IEEE, 2019c. doi: 10.1109/ICCV.2019.00041. URL <https://doi.org/10.1109/ICCV.2019.00041>.
- Jiaheng Wei, Hangyu Liu, Tongliang Liu, Gang Niu, Masashi Sugiyama, and Yang Liu. To smooth or not? when label smoothing meets noisy labels. *ArXiv preprint*, abs/2106.04149, 2021. URL <https://arxiv.org/abs/2106.04149>.
- Jiaheng Wei, Zhaowei Zhu, Hao Cheng, Tongliang Liu, Gang Niu, and Yang Liu. Learning with noisy labels revisited: A study using real-world human annotations. In *International Conference on Learning Representations, 2022*. URL <https://openreview.net/forum?id=TBWA6PLJZQm>.
- Quanming Yao, Hansi Yang, Bo Han, Gang Niu, and James Kwok. Searching to exploit memorization effect in learning from corrupted labels, 2019. URL <https://arxiv.org/abs/1911.02377>.
- Chiyuan Zhang, Samy Bengio, Moritz Hardt, Benjamin Recht, and Oriol Vinyals. Understanding deep learning requires rethinking generalization. In *5th International Conference on Learning Representations, ICLR 2017, Toulon, France, April 24-26, 2017, Conference Track Proceedings*. OpenReview.net, 2017. URL <https://openreview.net/forum?id=Sy8gdB9xx>.
- Xuan Zhang, Gaurav Kumar, Huda Khayrallah, Kenton Murray, Jeremy Gwinnup, Marianna J. Martindale, Paul McNamee, Kevin Duh, and Marine Carpuat. An empirical exploration of curriculum learning for neural machine translation. *ArXiv preprint*, abs/1811.00739, 2018. URL <https://arxiv.org/abs/1811.00739>.
- Zhilu Zhang and Mert R. Sabuncu. Generalized cross entropy loss for training deep neural networks with noisy labels. In Samy Bengio, Hanna M. Wallach, Hugo Larochelle, Kristen Grauman, Nicolò Cesa-Bianchi, and Roman Garnett (eds.), *Advances in Neural Information Processing Systems 31: Annual Conference on Neural Information Processing Systems 2018, NeurIPS 2018, December 3-8, 2018, Montréal, Canada*, pp. 8792–8802, 2018. URL <https://proceedings.neurips.cc/paper/2018/hash/f2925f97bc13ad2852a7a551802feea0-Abstract.html>.
- Tianyi Zhou, Shengjie Wang, and Jeff A. Bilmes. Robust curriculum learning: from clean label detection to noisy label self-correction. In *9th International Conference on Learning Representations, ICLR 2021, Virtual Event, Austria, May 3-7, 2021*. OpenReview.net, 2021a. URL <https://openreview.net/forum?id=lmTWnm3coJJ>.

Xiong Zhou, Xianming Liu, Junjun Jiang, Xin Gao, and Xiangyang Ji. Asymmetric loss functions for learning with noisy labels. In Marina Meila and Tong Zhang (eds.), *Proceedings of the 38th International Conference on Machine Learning, ICML 2021, 18-24 July 2021, Virtual Event*, volume 139 of *Proceedings of Machine Learning Research*, pp. 12846–12856. PMLR, 2021b. URL <http://proceedings.mlr.press/v139/zhou21f.html>.

## A EXTENDED REVIEW OF LOSS FUNCTIONS

Due to limited space, we only briefly describe typical robust loss functions in §3.1. As a general reference, here we provide a comprehensive review of loss functions related to the standard form Eq. (1). Similar to §3.1, we ignore the differences in constant scaling factors and additive bias. Loss functions and their sample-weighting functions are summarized in Table 6. We examine how hyperparameters affect their sample-weighting functions in Fig. 5.

### A.1 LOSS FUNCTIONS WITHOUT ROBUSTNESS GUARANTEES

#### Cross Entropy (CE)

$$L_{\text{CE}}(\mathbf{s}, y) = -\log p_y$$

is the standard loss function for classification.

#### Focal Loss (FL; Lin et al. 2017)

$$L_{\text{FL}}(\mathbf{s}, y) = -(1 - p_y)^q \log p_y$$

aims to address label imbalance when training object detection models. Both CE and FL are neither symmetric (Ma et al., 2020) nor asymmetric (Zhou et al., 2021b).

### A.2 SYMMETRIC LOSS FUNCTIONS

#### Mean Absolute Error (MAE; Ghosh et al. 2017)

$$L_{\text{MAE}}(\mathbf{s}, y) = \sum_{i=1}^k |\mathbb{I}(i = y) - p_i| = 2 - 2p_y \propto 1 - p_y$$

is a classic symmetric loss function, where  $\mathbb{I}(i = y)$  is the indicator function.

#### Reverse Cross Entropy (RCE; Wang et al. 2019c)

$$L_{\text{RCE}}(\mathbf{s}, y) = \sum_{i=1}^k p_i \log \mathbf{1}(i = y) = \sum_{i \neq y} p_i A = (1 - p_y)A \propto 1 - p_y = L_{\text{MAE}}(\mathbf{s}, y)$$

is equivalent to MAE in implementation, where  $\log 0$  is truncated to a negative constant  $A$  to avoid numerical overflow.

Ma et al. (2020) argued that any generic loss functions with  $L(\mathbf{s}, i) > 0, \forall i \in \{1..k\}$  can become symmetric by simply normalizing them. As an example,

#### Normalized Cross Entropy (NCE; Ma et al. 2020)

$$L_{\text{NCE}}(\mathbf{s}, y) = \frac{L_{\text{CE}}(\mathbf{s}, y)}{\sum_{i=1}^k L_{\text{CE}}(\mathbf{s}, i)} = \frac{-\log p_y}{\sum_{i=1}^k -\log p_i}$$

is a symmetric loss function. However, NCE does not follow the standard form of Eq. (1) as it additionally depends on  $p_i, i \neq y$ . It involves an additional regularizer, thus being more relevant to discussions in Appendix A.5.

### A.3 ASYMMETRIC LOSS FUNCTIONS

Zhou et al. (2021b) derived the asymmetric condition for noise robustness and propose numerous asymmetric loss functions:

#### Asymmetric Generalized Cross Entropy (AGCE)

$$L_{\text{AGCE}}(\mathbf{s}, y) = \frac{(a + 1) - (a + p_y)^q}{q}$$

Name	Function	Sample Weight $w$	Constraints
CE	$-\log p_y$	$1 - p_y$	
FL	$-(1 - p_y)^q \log p_y$	$(1 - p_y)^q (1 - p_y - qp_y \log p_y)$	$q > 0$
MAE/RCE	$1 - p_y$	$p_y(1 - p_y)$	
AUL	$\frac{(a+1)-(a+p_y)^q}{q}$	$p_y(1 - p_y)(a - p_y)^{q-1}$	$a > 1, q > 0$
AGCE	$\frac{(a-p_y)^q - (a-1)^q}{q}$	$p_y(a + p_y)^{q-1}(1 - p_y)$	$a > 0, q > 0$
AEL	$e^{-p_y/q}$	$\frac{1}{q} p_y(1 - p_y)e^{-p_y/q}$	$q > 0$
GCE	$(1 - p_y^q)/q$	$p_y^q(1 - p_y)$	$0 < q \leq 1$
SCE	$-(1 - q) \log p_y + q(1 - p_y)$	$(1 - q + q \cdot p_y)(1 - p_y)$	$0 < q < 1$
TCE	$\sum_{i=1}^q (1 - p_y)^i / i$	$p_y \sum_{i=1}^q (1 - p_y)^i$	$q \geq 1$

Table 6: Expressions, constraints of hyperparameters and sample-weighting functions of loss functions reviewed in Appendix A that follow the standard form Eq. (1).

where  $a > 0$  and  $q > 0$ . It is asymmetric when  $\mathbb{I}(q \leq 1)(\frac{a+1}{a})^{1-q} + \mathbb{I}(q > 1) \leq 1/\tilde{r}$ .

#### Asymmetric Unhinged Loss (AUL)

$$L_{\text{AUL}}(\mathbf{s}, y) = \frac{(a - p_y)^q - (a - 1)^q}{q}$$

where  $a > 1$  and  $q > 0$ . It is asymmetric when  $\mathbb{I}(q \leq 1)(\frac{a}{a-1})^{q-1} + \mathbb{I}(q > 1) \leq 1/\tilde{r}$ .

#### Asymmetric Exponential Loss (AEL)

$$L_{\text{AEL}}(\mathbf{s}, y) = e^{-p_y/q}$$

where  $q > 0$ . It is asymmetric when  $e^{1/q} \leq 1/\tilde{r}$ .

### A.4 COMBINED LOSS FUNCTIONS

#### Generalized Cross Entropy (GCE; Zhang & Sabuncu 2018)

$$L_{\text{GCE}}(\mathbf{s}, y) = \frac{1 - p_y^q}{q}$$

can be viewed as a smooth interpolation between CE and MAE, where  $0 < q \leq 1$ . CE or MAE can be recovered by setting  $q \rightarrow 0$  or  $q = 1$ .

#### Symmetric Cross Entropy (SCE; Wang et al. 2019c)

$$\begin{aligned} L_{\text{SCE}}(\mathbf{s}, y) &= a \cdot L_{\text{CE}}(\mathbf{s}, y) + b \cdot L_{\text{RCE}}(\mathbf{s}, y) \\ &\propto (1 - q) \cdot (-\log p_i) + q \cdot (1 - p_i) \end{aligned}$$

is a weighted average of CE and RCE (MAE), where  $a > 0$ ,  $b > 0$ , and  $0 < q < 1$ .

#### Taylor Cross Entropy (TCE; Feng et al. 2020)

$$L_{\text{TCE}}(\mathbf{s}, y) = \sum_{i=1}^q \frac{(1 - p_y)^i}{i}$$

is derived from Taylor series of the log function. It reduces to MAE when  $q = 1$ . Interestingly, the summand of TCE  $(1 - p_y)^i / i$  with  $i > 2$  is proportional to AUL with  $a = 1$  and  $q = i$ . Thus TCE can be viewed as a combination of symmetric and asymmetric loss functions.

#### Active-Passive Loss (APL; Ma et al. 2020)

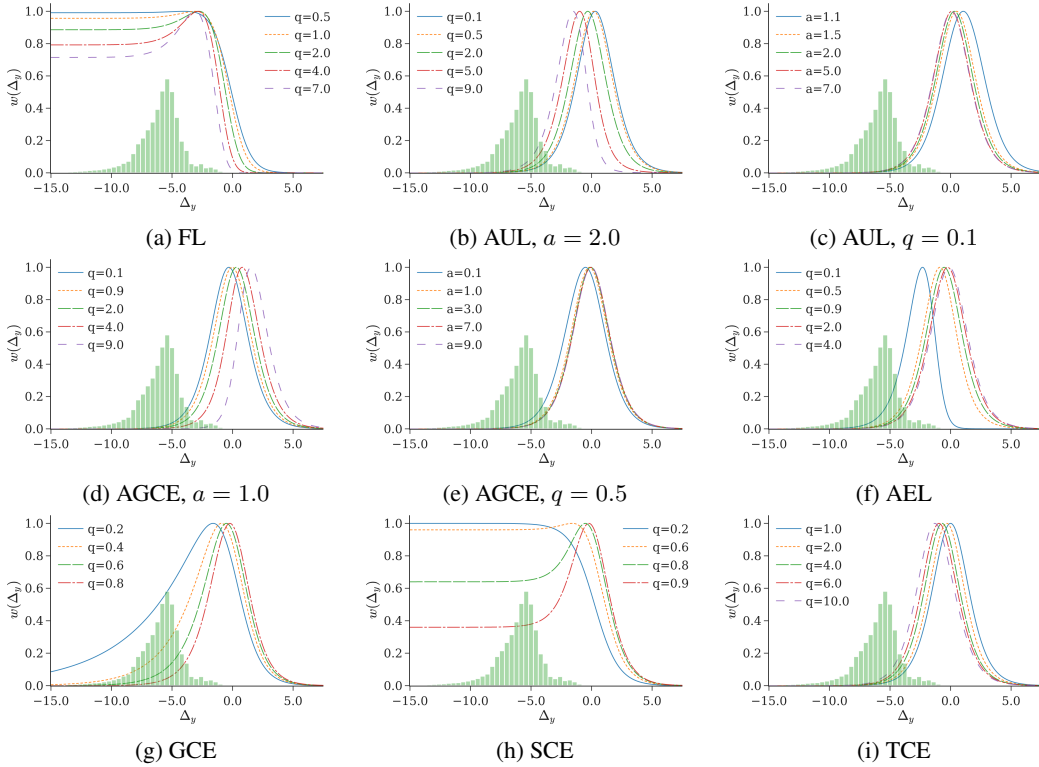


Figure 5: How hyperparameters affect the sample-weighting functions in Table 6. The initial  $\Delta_y$  distributions of CIFAR100 extracted with a randomly initialized model are included as reference.

Ma et al. (2020) propose weighted combinations of active and passive loss functions. We include NCE+MAE as an example:

$$\begin{aligned} L_{\text{NCE+MAE}}(\mathbf{s}, y) &= a \cdot L_{\text{NCE}}(\mathbf{s}, y) + b \cdot L_{\text{MAE}}(\mathbf{s}, y) \\ &\propto (1 - q) \cdot \frac{-\log p_y}{\sum_{i=1}^k -\log p_i} + q \cdot (1 - p_y) \end{aligned}$$

where  $a > 0$ ,  $b > 0$ , and  $0 < q < 1$ .

#### A.5 LOSS FUNCTIONS WITH ADDITIONAL REGULARIZERS

We additionally review loss functions that implicitly involve a regularizer and a primary loss function following the standard form Eq. (1). See Table 7 for a summary. In addition to the sample-weighting curriculums implicitly defined by the primary loss function, the additional regularizer complicates the analysis of the training dynamics. We leave investigations on how these regularizers affect noise robustness for future work.

**Mean Square Error (MSE; Ghosh et al. 2017)**

$$\begin{aligned} L_{\text{MSE}}(\mathbf{s}, y) &= \sum_{i=1}^k (\mathbb{I}(i = y) - p_i)^2 = 1 - 2p_y + \sum_{i=1}^k p_i^2 \\ &\propto 1 - p_y + \frac{1}{2} \cdot \sum_{i=1}^k p_i^2 = L_{\text{MAE}}(\mathbf{s}, y) + \alpha \cdot R_{\text{MSE}}(\mathbf{s}) \end{aligned}$$

is more robust than CE (Ghosh et al., 2017), where  $\alpha = 0.5$  and the regularizer

$$R_{\text{MSE}}(\mathbf{s}) = \sum_{i=1}^k p_i^2 \quad (5)$$

increases the entropy of the softmax output. We can generalize  $\alpha$  to a hyperparameter, making MSE a combination of MAE and an entropy regularizer  $R_{\text{MSE}}$ .



Name	Original	Primary Loss	Regularizer
MSE	$1 - 2p_y + \sum_{i=1}^k p_i^2$	$1 - p_y$	$\sum_{i=1}^k p_i^2$
PL(CR)	$-\log p_y + \log p_{y_n \mathbf{x}_m}$	$-\log p_y$	$\sum_{i=1}^k P(\tilde{y} = i) \log p_i$
CE+GLS	$-\sum_{i=1}^k [\mathbb{I}(i = y)(1 - \alpha) + \frac{\alpha}{k}] \log p_i$	$-\log p_y$	$\pm \sum_{i=1}^k \frac{1}{k} \log p_i$
NCE	$-\log p_y / (\sum_{i=1}^k -\log p_i)$	$-\gamma_{\text{NCE}} \cdot \log p_i$	$\sum_{i=1}^k \frac{1}{k} \log p_i$

Table 7: Original expressions, primary loss functions in the standard form Eq. (1) and regularizers for loss functions reviewed in Appendix A.5. We view PL in its expectation to derive its regularizer.  $p_{y_n|\mathbf{x}_m}$  is the softmax probability of a random label  $y_n$  with a random input  $\mathbf{x}_m$  sampled from the noisy data.  $\gamma_{\text{NCE}} = 1/(\sum_{i=1}^k -\log p_i)$  is a scalar wrapped with the stop-gradient operator.

#### Peer Loss (PL; Liu & Guo 2020)

$$L_{\text{PL}}(\mathbf{s}, y) = L(\mathbf{s}, y) - L(\mathbf{s}_n, y_m)$$

makes a generic loss function  $L(\mathbf{s}, y)$  robust against label noise, where  $\mathbf{s}_n$  denotes the score of an input  $\mathbf{x}_n$  and  $y_m$  a label, both randomly sampled from the noisy data. Its noise robustness is theoretically established for binary classification and extended to multi-class setting (Liu & Guo, 2020).

#### Confidence Regularizer (CR; Cheng et al. 2021)

$$R_{\text{CR}}(\mathbf{s}) = -\mathbb{E}_{\tilde{y}}[L(\mathbf{s}, \tilde{y})]$$

is shown (Cheng et al., 2021) to be the regularizer induced by PL in expectation. Substituting  $L$  with cross entropy leads to

$$R_{\text{CR}}(\mathbf{s}) = -\mathbb{E}_{\tilde{y}}[-\log p_{\tilde{y}}] = \sum_{i=1}^k P(\tilde{y} = i) \log p_i \quad (6)$$

Minimizing  $R_{\text{CR}}(\mathbf{s})$  thus makes the softmax output distribution  $\mathbf{p}$  deviate from the prior label distribution of the noisy dataset  $P(\tilde{y} = i)$ , reducing the entropy of the softmax output.

#### Generalized Label Smoothing (GLS; Wei et al. 2021)

Lukasik et al. (2020) show that label smoothing (LS; Szegedy et al. 2016) can mitigate overfitting with label noise, which is later extended to GSL. Cross entropy with GLS is

$$\begin{aligned} L_{\text{CE+GLS}}(\mathbf{s}, y) &= \sum_{i=1}^k -[\mathbb{I}(i = y)(1 - \alpha) + \frac{\alpha}{k}] \log p_i \\ &= -(1 - \alpha) \log p_y - \alpha \cdot \frac{1}{k} \sum_{i=1}^k \log p_i \\ &\propto -\log p_y - \frac{\alpha}{1 - \alpha} \cdot \frac{1}{k} \sum_{i=1}^k \log p_i = L_{\text{CE}}(\mathbf{s}, y) + \alpha' \cdot R_{\text{GLS}}(\mathbf{s}) \end{aligned}$$

where  $\alpha' = \alpha/(1 - \alpha)$ , has regularizer  $R_{\text{GLS}}$

$$R_{\text{GLS}}(\mathbf{s}) = -\sum_{i=1}^k \frac{1}{k} \log p_i \quad (7)$$

With  $\alpha' > 0$ ,  $R_{\text{GLS}}$  corresponds to the original label smoothing, which increases the entropy of softmax outputs. In contrast,  $\alpha' < 0$  corresponding to negative label smoothing (Wei et al., 2021), which decreases the output entropy similar to  $R_{\text{CR}}$ .

## A.5.1 DERIVATIONS FOR NCE

**Deriving Eq. (2)** With equivalent derivatives, since

$$\begin{aligned}\nabla_{\mathbf{s}} L_{\text{NCE}}(\mathbf{s}, y) &= \frac{\nabla_{\mathbf{s}} L_{\text{CE}}(\mathbf{s}, y) \cdot \left[ \sum_{i=1}^k L_{\text{CE}}(\mathbf{s}, i) \right] - \nabla_{\mathbf{s}} \left[ \sum_{i=1}^k L_{\text{CE}}(\mathbf{s}, i) \right] \cdot L_{\text{CE}}(\mathbf{s}, y)}{\left[ \sum_{i=1}^k L_{\text{CE}}(\mathbf{s}, i) \right]^2} \\ &= \frac{1}{\sum_{i=1}^k L_{\text{CE}}(\mathbf{s}, i)} \left\{ \nabla_{\mathbf{s}} L_{\text{CE}}(\mathbf{s}, y) + \frac{k L_{\text{CE}}(\mathbf{s}, y)}{\sum_{i=1}^k L_{\text{CE}}(\mathbf{s}, i)} \cdot \nabla_{\mathbf{s}} \left[ \sum_{i=1}^k -\frac{1}{k} L_{\text{CE}}(\mathbf{s}, i) \right] \right\} \\ &= \gamma_{\text{NCE}} \cdot [\nabla_{\mathbf{s}} L_{\text{CE}}(\mathbf{s}, y) + \epsilon_{\text{NCE}} \cdot \nabla_{\mathbf{s}} R_{\text{NCE}}(\mathbf{s})],\end{aligned}$$

NCE can be rewritten as

$$L_{\text{NCE}}(\mathbf{s}, y) = \gamma_{\text{NCE}} \cdot L_{\text{CE}}(\mathbf{s}, y) + \gamma_{\text{NCE}} \cdot \epsilon_{\text{NCE}} \cdot R_{\text{NCE}}(\mathbf{s})$$

where  $\gamma_{\text{NCE}} = 1/(\sum_{i=1}^k -\log p_i)$  and  $\epsilon_{\text{NCE}} = k(-\log p_y)/(\sum_{i=1}^k -\log p_i)$  are scalar weights wrapped with the stop-gradient operator as discussed in §4.1. The regularizer

$$R_{\text{NCE}}(\mathbf{s}) = \sum_{i=1}^k \frac{1}{k} \log p_i$$

has a form similar to  $R_{\text{GLS}}$ .

**Deriving  $\hat{w}_{\text{NCE}}$  of Eq. (3)** Here we derive the upperbound of  $\|\nabla_{\mathbf{s}} L_{\text{NCE}}(\mathbf{s}, y)\|_1$  discussed in §4.1:

$$\begin{aligned}\|\nabla_{\mathbf{s}} L_{\text{NCE}}(\mathbf{s}, y)\|_1 &\leq \gamma_{\text{NCE}} \cdot (\|\nabla_{\mathbf{s}} L_{\text{CE}}(\mathbf{s}, y)\|_1 + \epsilon_{\text{NCE}} \cdot \|\nabla_{\mathbf{s}} R_{\text{NCE}}(\mathbf{s})\|_1) \\ &\leq \gamma_{\text{NCE}} \cdot \left( \|\nabla_{\mathbf{s}} L_{\text{CE}}(\mathbf{s}, y)\|_1 + \epsilon_{\text{NCE}} \cdot \frac{1}{k} \sum_{i=1}^k \|\nabla_{\mathbf{s}} L_{\text{CE}}(\mathbf{s}, i)\|_1 \right) \\ &= \gamma_{\text{NCE}} \cdot \left( w_{\text{CE}} \cdot \|\nabla_{\mathbf{s}} \Delta_y\|_1 + \epsilon_{\text{NCE}} \cdot \frac{1}{k} \sum_{i=1}^k w_{\text{CE}} \cdot \|\nabla_{\mathbf{s}} \Delta_i\|_1 \right) \\ &= 2\gamma_{\text{NCE}} \cdot w_{\text{CE}} (1 + \epsilon_{\text{NCE}}) \\ &= \hat{w}_{\text{NCE}}\end{aligned}$$

The derivation is based on the inequality  $|x \pm y| \leq |x| + |y|$  and the fact that  $\|\nabla_{\mathbf{s}} \Delta_i\|_1 = 2$ . The latter can be proved by straightforward calculations. Given

$$\frac{\partial \Delta_i}{\partial s_j} = \begin{cases} 1, & j = i \\ -\frac{e^{s_j}}{\sum_{k \neq i} e^{s_k}} = -\frac{p_j}{1-p_i}, & j \neq i \end{cases}$$

we then have

$$\|\nabla_{\mathbf{s}} \Delta_i\|_1 = \sum_j \left| \frac{\partial \Delta_i}{\partial s_j} \right| = 1 + \sum_{j \neq i} \frac{p_j}{1-p_i} = 1 + 1 = 2$$

## B DETAILED EXPERIMENTAL SETTINGS

**Label noise** The synthetic noisy labels are generated following (Ma et al., 2020; Zhou et al., 2021b; Patrini et al., 2017). For symmetric label noise, the training labels are randomly flipped to a different class with probabilities  $\eta \in \{0.2, 0.4, 0.6, 0.8\}$ . Asymmetric label noise is generated from a class-dependent flipping pattern. On CIFAR100, the 100 classes are grouped into 20 super-classes, each having 5 sub-classes. Each class is flipped within the same super-class into the next in a circular fashion. The flip probabilities are  $\eta \in \{0.1, 0.2, 0.3, 0.4\}$ . Human label noise for CIFAR10/100 are adopted from Wei et al. (2022). We use the “worst” labels of CIFAR10-N and the “fine” labels of CIFAR100-N, both leading to  $\eta = 0.4$ .

**Models and hyperparameters** We use a 4-layer CNN for MNIST, an 8-layer CNN for CIFAR10, a ResNet-34 (He et al., 2016) for CIFAR100, and a ResNet-50 (He et al., 2016) for WebVision, all with batch normalization (Ioffe & Szegedy, 2015). Data augmentation on CIFAR10/100 include random

	SCE	GCE	NCE+MAE	AUL	AGCE	AUL <sup>†</sup>	AGCE <sup>†</sup>
<i>a</i>	/	/	/	1.1	0.1	3.0	1.6
<i>q</i>	0.7	0.3	0.3	5.0	0.1	0.7	2.0

Table 8: Hyperparameters of different loss functions for results in §5.1 and Appendix C.1. They are tuned on CIFAR100 without label noise. Settings with inferior hyperparameters are denoted with †.

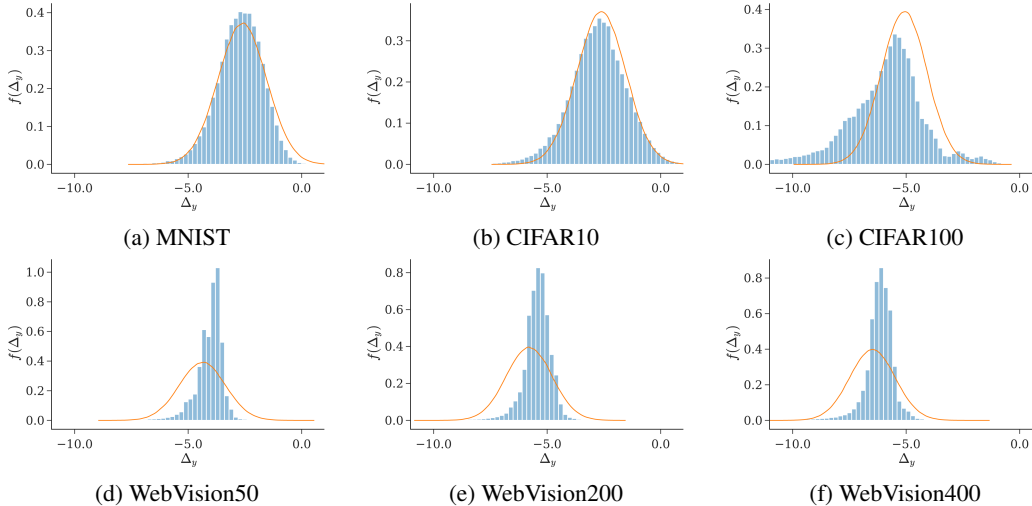


Figure 6: Comparisons between simulated and real  $\Delta_y$  distributions at initialization. The simulations are based on the assumption that class scores follow normal distribution  $s_i \sim \mathcal{N}(0, 1)$  at initialization and plotted as curves. Real distributions are extracted with randomly initialized models and plotted as histograms. The vertical axis denotes probability density  $f(\Delta_y)$ .

width/height shift and horizontal flip. On WebVision, we additionally include random cropping and color jittering. Without further specifications, all models are trained using SGD with momentum 0.9 and batch size 128 for 50, 120, 200 and 250 epochs on MNIST, CIFAR10, CIFAR100 and WebVision, respectively. Learning rates with cosine annealing are 0.01 on MNIST and CIFAR10, 0.1 on CIFAR100, and 0.2 on WebVision. Weight decays are  $10^{-3}$  on MNIST,  $10^{-4}$  on CIFAR10,  $10^{-5}$  on CIFAR100 and  $3 \times 10^{-5}$  on WebVision. All loss functions are normalized to have unit maximum in sample weights, which is different from (Ma et al., 2020). Hyperparameters of loss functions are listed in Tables 8 and 12 for different experiments.

## C ADDITIONAL RESULTS TO UNDERSTAND ROBUST LOSS FUNCTIONS

We complement §5 in the main text with detailed derivations and additional results. Appendix C.1 extends discussions in §5.1 while Appendix C.2 extends §5.2

### C.1 UNDERSTANDING UNDERFITTING OF ROBUST LOSS FUNCTIONS

**Hyperparameters** We list the hyperparameters tuned on CIFAR100 without label noise in Table 8 for experiments in §5.1 and Appendix C.1.

**Simulated  $\Delta_y$  approximate real settings.** We compare the simulated  $\Delta_y$  distributions based on our assumptions in §5.1 to distributions of real datasets at initialization in Fig. 6. The expectations of simulated  $\Delta_y$  follow real settings, which supports the analysis in §5.1.

Settings	Clean	Symmetric				Asymmetric				Human
	0.0	0.2	0.4	0.6	0.8	0.1	0.2	0.3	0.4	0.4
MAE shift	2.0	2.6	3.0	4.0	4.0	2.6	2.6	3.0	3.0	2.6
MAE scale	2.0	2.6	2.6	3.0	4.0	2.6	2.6	3.0	3.0	2.6
AGCE shift	4.0	4.0	4.0	5.0	5.0	4.0	4.0	4.0	4.0	4.0
AGCE scale	2.6	3.0	4.0	5.0	5.0	3.0	3.0	3.0	3.0	4.0

Table 9: Hyperparameter  $\tau$  of  $w^*(\Delta_y)$  and  $w^+(\Delta_y)$  for different noise settings on CIFAR100. For reference,  $\mathbb{E}[\Delta_y] = 5.097$  on CIFAR100 and  $\mathbb{E}[\Delta_y] = 2.717$  on CIFAR10. Better performance can be achieved with a more thorough hyperparameter search.

Loss	Clean	Symmetric Noise (Noise Rate $\eta$ )			
	$\eta = 0$	$\eta = 0.2$	$\eta = 0.4$	$\eta = 0.6$	$\eta = 0.8$
CE <sup>‡</sup>	71.33 $\pm$ 0.43	56.51 $\pm$ 0.39	39.92 $\pm$ 0.10	21.39 $\pm$ 1.17	7.59 $\pm$ 0.20
GCE <sup>‡</sup>	63.09 $\pm$ 1.39	61.57 $\pm$ 1.06	56.11 $\pm$ 1.35	45.28 $\pm$ 0.61	17.42 $\pm$ 0.06
NCE <sup>‡</sup>	29.96 $\pm$ 0.73	25.27 $\pm$ 0.32	19.54 $\pm$ 0.52	13.51 $\pm$ 0.65	8.55 $\pm$ 0.37
NCE+AUL <sup>‡</sup>	68.96 $\pm$ 0.16	65.36 $\pm$ 0.20	59.25 $\pm$ 0.23	46.34 $\pm$ 0.21	23.03 $\pm$ 0.64
AGCE	49.27 $\pm$ 1.03	49.17 $\pm$ 2.15	47.76 $\pm$ 1.75	38.17 $\pm$ 1.43	16.03 $\pm$ 0.59
AGCE shift	69.39 $\pm$ 0.84	62.81 $\pm$ 0.42	48.21 $\pm$ 1.06	36.70 $\pm$ 2.89	14.49 $\pm$ 0.17
AGCE scale	70.57 $\pm$ 0.62	64.73 $\pm$ 0.98	56.69 $\pm$ 0.33	39.02 $\pm$ 1.20	14.64 $\pm$ 0.79
MAE	3.69 $\pm$ 0.59	2.92 $\pm$ 0.46	1.29 $\pm$ 0.50	2.27 $\pm$ 1.24	1.00 $\pm$ 0.00
MAE shift	69.02 $\pm$ 0.78	59.75 $\pm$ 0.84	44.60 $\pm$ 0.24	24.27 $\pm$ 0.26	8.08 $\pm$ 0.26
MAE scale	<b>70.97 <math>\pm</math> 0.41</b>	<b>66.83 <math>\pm</math> 0.84</b>	<b>60.57 <math>\pm</math> 1.04</b>	<b>49.23 <math>\pm</math> 1.22</b>	<b>24.44 <math>\pm</math> 0.73</b>

Table 10: Addition results to Table 3 with more symmetric label noise rates on CIFAR100.

**Derivation of Eq. (4)** Assume that class scores  $s_i$  at *initialization* are i.i.d. normal variables, i.e.,  $s_i \sim \mathcal{N}(\mu, \sigma)$ ,

$$\begin{aligned}
\mathbb{E}(\Delta_y) &= \mathbb{E}[s_y - \log \sum_{i \neq y} e^{s_i}] = \mu - \mathbb{E}[\log \sum_{i \neq y} e^{s_i}] \\
&\approx_1 \mu - \log \mathbb{E}[\sum_{i \neq y} e^{s_i}] + \frac{\mathbb{V}[\sum_{i \neq y} e^{s_i}]}{2\mathbb{E}[\sum_{i \neq y} e^{s_i}]^2} \\
&=_2 \mu - \log\{(k-1)\mathbb{E}[e^{s_y}]\} + \frac{(k-1)\mathbb{V}[e^{s_y}]}{2\{(k-1)\mathbb{E}[e^{s_y}]\}^2} \\
&=_3 \mu - \log[(k-1)e^{\mu+\sigma^2/2}] + \frac{(k-1)(e^{\sigma^2}-1)e^{2\mu+\sigma^2}}{2[(k-1)e^{\mu+\sigma^2/2}]^2} \\
&= -\log(k-1) - \sigma^2/2 + \frac{e^{\sigma^2}-1}{2(k-1)}
\end{aligned}$$

where  $\approx_1$  follows the approximation with Taylor expansion  $\mathbb{E}[\log X] \approx \log \mathbb{E}[X] - \mathbb{V}[X]/(2\mathbb{E}[X]^2)$  (Teh et al., 2006),  $=_2$  utilizes properties of sum of log-normal variables (Cobb et al., 2012), and  $=_3$  substitutes  $\mathbb{E}[e^{s_y}]$  and  $\mathbb{V}[e^{s_y}]$  with expressions for log-normal distributions.

### C.1.1 ADDRESSING UNDERFITTING FROM MARGINAL INITIAL SAMPLE WEIGHTS

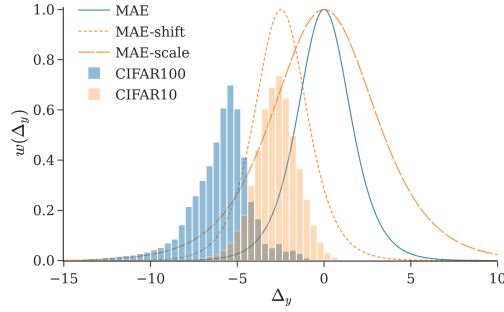
**Hyperparameter  $\tau$  for different settings** The hyperparameter  $\tau$  controlling the shape of modified sample-weighting functions  $w^+(\Delta_y)$  and  $w^*(\Delta_y)$  can affect the noise robustness. Thus we tune  $\tau$  for the best performance under different noise types and noise rates, which are listed in Table 9.

**Additional results with  $w^*(\Delta_y)$  and  $w^+(\Delta_y)$ .** We report additional results under symmetric and asymmetric label noise with diverse noise rates  $\eta$  in Table 10 and Table 11, respectively. Performance of MAE and AGCE gets substantially improved with  $w^*(\Delta_y)$  and  $w^+(\Delta_y)$ .

**Visualization of  $w^*(\Delta_y)$  and  $w^+(\Delta_y)$ .** In Fig. 7 we visualize the shifted and scaled sample-weighting functions of MAE on CIFAR100. Although both achieve the same initial sample weights

Loss	Clean	Asymmetric Noise (Noise Rate $\eta$ )			
	$\eta = 0$	$\eta = 0.1$	$\eta = 0.2$	$\eta = 0.3$	$\eta = 0.4$
CE <sup>‡</sup>	71.33 $\pm$ 0.43	64.85 $\pm$ 0.37	58.11 $\pm$ 0.32	50.68 $\pm$ 0.55	40.17 $\pm$ 1.31
GCE <sup>‡</sup>	63.09 $\pm$ 1.39	63.01 $\pm$ 1.01	59.35 $\pm$ 1.10	53.83 $\pm$ 0.64	40.91 $\pm$ 0.57
NCE <sup>‡</sup>	29.96 $\pm$ 0.73	27.59 $\pm$ 0.54	25.75 $\pm$ 0.50	24.28 $\pm$ 0.80	20.64 $\pm$ 0.40
NCE+AUL <sup>‡</sup>	68.96 $\pm$ 0.16	66.62 $\pm$ 0.09	63.86 $\pm$ 0.18	50.38 $\pm$ 0.32	38.59 $\pm$ 0.48
AGCE	49.27 $\pm$ 1.03	47.53 $\pm$ 0.73	46.77 $\pm$ 2.37	39.82 $\pm$ 2.70	33.40 $\pm$ 1.57
AGCE shift	69.39 $\pm$ 0.84	63.03 $\pm$ 0.42	55.84 $\pm$ 0.78	49.05 $\pm$ 0.81	40.76 $\pm$ 0.74
AGCE scale	70.57 $\pm$ 0.62	67.13 $\pm$ 0.60	59.71 $\pm$ 0.10	48.23 $\pm$ 0.29	39.71 $\pm$ 0.17
MAE	3.69 $\pm$ 0.59	3.59 $\pm$ 0.56	3.19 $\pm$ 0.98	2.11 $\pm$ 1.93	2.53 $\pm$ 1.34
MAE shift	68.57 $\pm$ 0.54	63.44 $\pm$ 0.32	56.47 $\pm$ 0.48	48.79 $\pm$ 1.22	39.83 $\pm$ 0.18
MAE scale	<b>70.97 <math>\pm</math> 0.41</b>	<b>69.50 <math>\pm</math> 0.24</b>	<b>64.80 <math>\pm</math> 0.49</b>	<b>59.04 <math>\pm</math> 1.52</b>	<b>44.48 <math>\pm</math> 1.05</b>

Table 11: Addition results to Table 3 with more asymmetric label noise rates on CIFAR100.

Figure 7: Shifted, scaled and the vanilla sample-weighting functions of MAE on CIFAR100.  $\tau$  equals  $|\mathbb{E}[\Delta_y]|$  on CIFAR10. We include the initial  $\Delta_y$  distributions of CIFAR10/100 extracted with a randomly initialized model as reference.

at  $|\mathbb{E}[\Delta_y]|$  of CIFAR100,  $w^+(\Delta_y)$  diminishes much faster as  $\Delta_y$  increases, leading to insufficient learning of training samples, which can explain its inferior performance in Tables 3, 4, 10 and 11.

**Robustness of loss functions from  $w^*(\Delta_y)$  and  $w^+(\Delta_y)$ .** Our proposed  $w^*(\Delta_y)$  and  $w^+(\Delta_y)$  aim to address the underfitting issue of robust loss functions with marginal initial sample weights. They modify  $p_y$  into

$$p_y^* = \frac{1}{e^{-(\Delta_y/|\mathbb{E}[\Delta_y]|\cdot\tau)} + 1} = \frac{1}{e^{-(\Delta_y\cdot\alpha)} + 1}$$

and

$$p_y^* = \frac{1}{e^{-(\Delta_y+|\mathbb{E}[\Delta_y]|\cdot\tau)} + 1} = \frac{1}{e^{-(\Delta_y+\beta)} + 1},$$

where  $\alpha = \tau/|\mathbb{E}[\Delta_y]|$  and  $\beta = |\mathbb{E}[\Delta_y]| - \tau$ , which induces new loss functions  $L^*(s, y) = l(p_y^*)$  and  $L^+(s, y) = l(p_y^+)$ , respectively. Commonly  $\alpha < 1$  and  $\beta > 0$  since a small  $\tau$  leads to large initial sample weights and underfitting results from small  $|\mathbb{E}[\Delta_y]|$ . Notably,  $\tau$  can determine the robustness of the induced loss functions. As shown in Table 9, a larger noise rate  $\eta$  requires a larger  $\tau$  for better performance, which assigns less weights to samples with small  $\Delta_y$  in general. However, our preliminary exploration find no straightforward derivation from  $L(s, y)$  being symmetric/asymmetric to  $L^*(s, y)$  and  $L^+(s, y)$  being symmetric/asymmetric. We leave the theoretical discussions to future work.

## C.2 NOISE ROBUSTNESS OF LOSS FUNCTIONS

**Computation of  $\bar{w}_{\text{clean}}$  and  $\bar{w}_{\text{noise}}$  for snr in Table 5** The average weight for clean samples, adjusted by the learning rate at each step  $\alpha_t$ , can be

$$\bar{w}_{\text{clean}} = \frac{\sum_{i,t} \alpha_t \cdot \mathbb{I}(\tilde{y}_{i,t} = y_{i,t}) w_{i,t}}{\sum_{i,t} \alpha_t \cdot \mathbb{I}(\tilde{y}_{i,t} = y_{i,t})}$$

	AUL	AGCE	GCE	SCE
$a$	2.0	3.0	/	/
$q$	2.0	4.0	0.4	0.95

Table 12: Hyperparameters of different loss functions for results in §5.2 and Appendix C.2. They are selected for broad coverage of shapes, scales and horizontal locations of sample-weighting functions instead of optimal performance on CIFAR10.

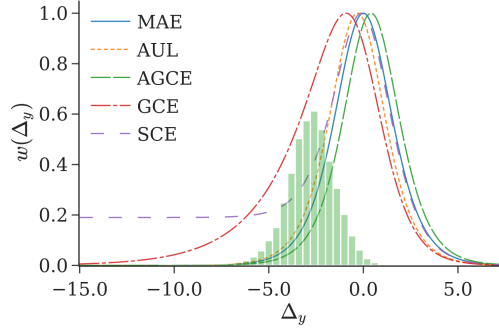


Figure 8: Plots of sample-weighting functions of loss functions used in Table 5 with hyperparameters in Table 8.

where  $w_{i,t}$  denotes the weight of  $i$ -th sample of the batch at step  $t$ ,  $\tilde{y}_{i,t}$  is the potentially corrupted noisy label and  $y_{i,t}$  the uncorrupted label. Similarly, for noisy samples,

$$\bar{w}_{\text{noise}} = \frac{\sum_{i,t} \alpha_t \cdot \mathbb{I}(\tilde{y}_{i,t} \neq y_{i,t}) w_{i,t}}{\sum_{i,t} \alpha_t \cdot \mathbb{I}(\tilde{y}_{i,t} \neq y_{i,t})}$$

**Hyperparameters** We list the hyperparameters for different loss functions in Table 12 for results in §5.2 and Appendix C.2. In Fig. 8, we plot the sample-weighting functions of different loss functions.

**Changes of  $\Delta_y$  distributions with different label noise and loss functions** Complementing Fig. 3, in Fig. 9 we plot how distributions of  $\Delta_y$  change during training on CIFAR10 with additional types of label noise using hyperparameters in Table 12. They follow similar trends as in Fig. 3, thus supporting analysis in §5.2. As MAE is not robust against asymmetric label noise with high  $\eta$  (Ghosh et al., 2017), it results in inferior performance. We also include results with additional loss functions in Fig. 10. Since optimal hyperparameters will result in similar sample-weighting functions, we choose hyperparameters for broad coverage of  $w(\Delta_y)$  to better understand how they affect robustness.

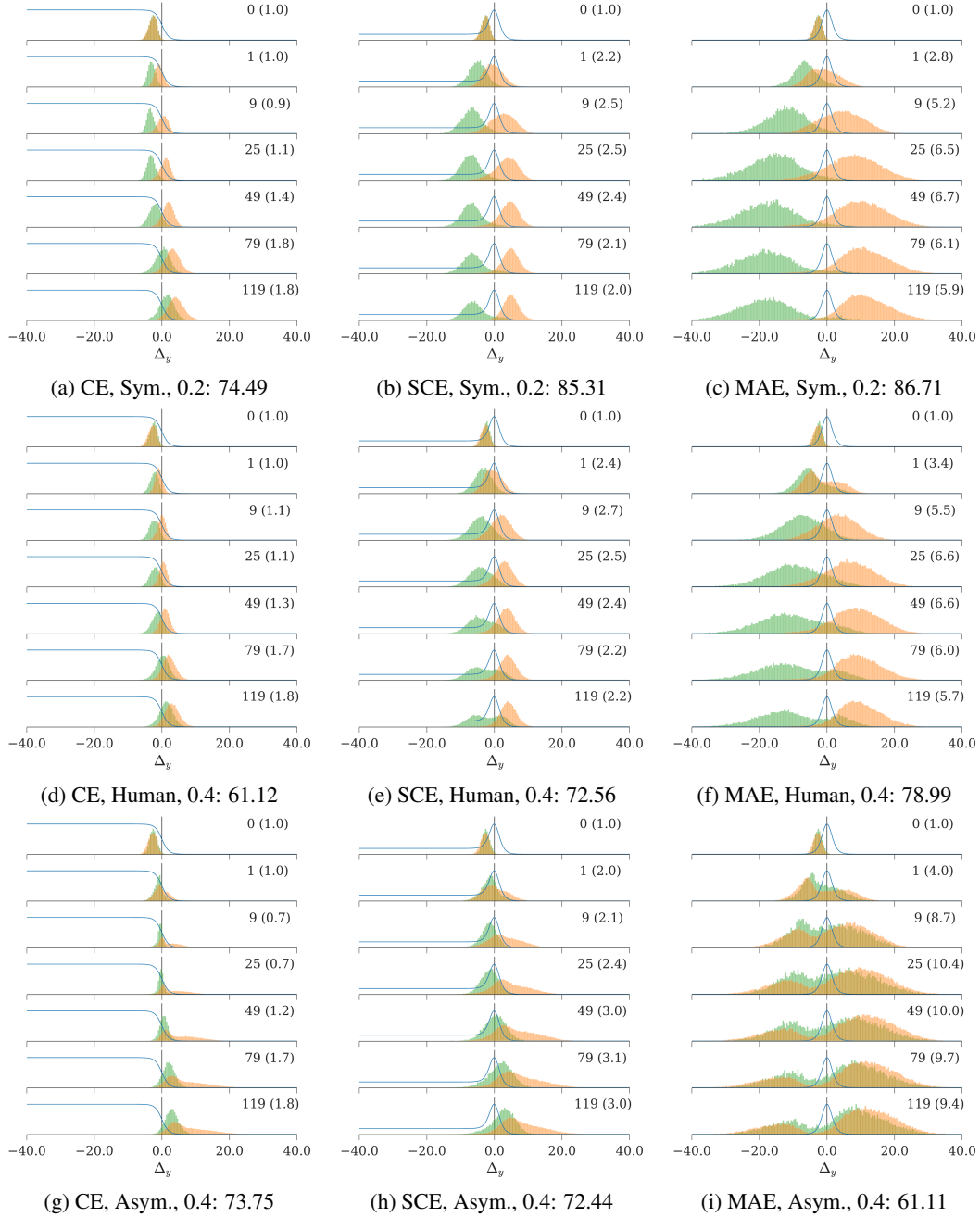


Figure 9: Additional results to Fig. 3 with different label noise: (a-c) symmetric label noise with  $\eta = 0.2$ ; (d-f) human label noise with  $\eta = 0.4$ ; (g-i) asymmetric label noise with  $\eta = 0.4$ . Noisy samples are colored green (on the left) and clean samples are orange (on the right). Test accuracies are included in the caption for reference.

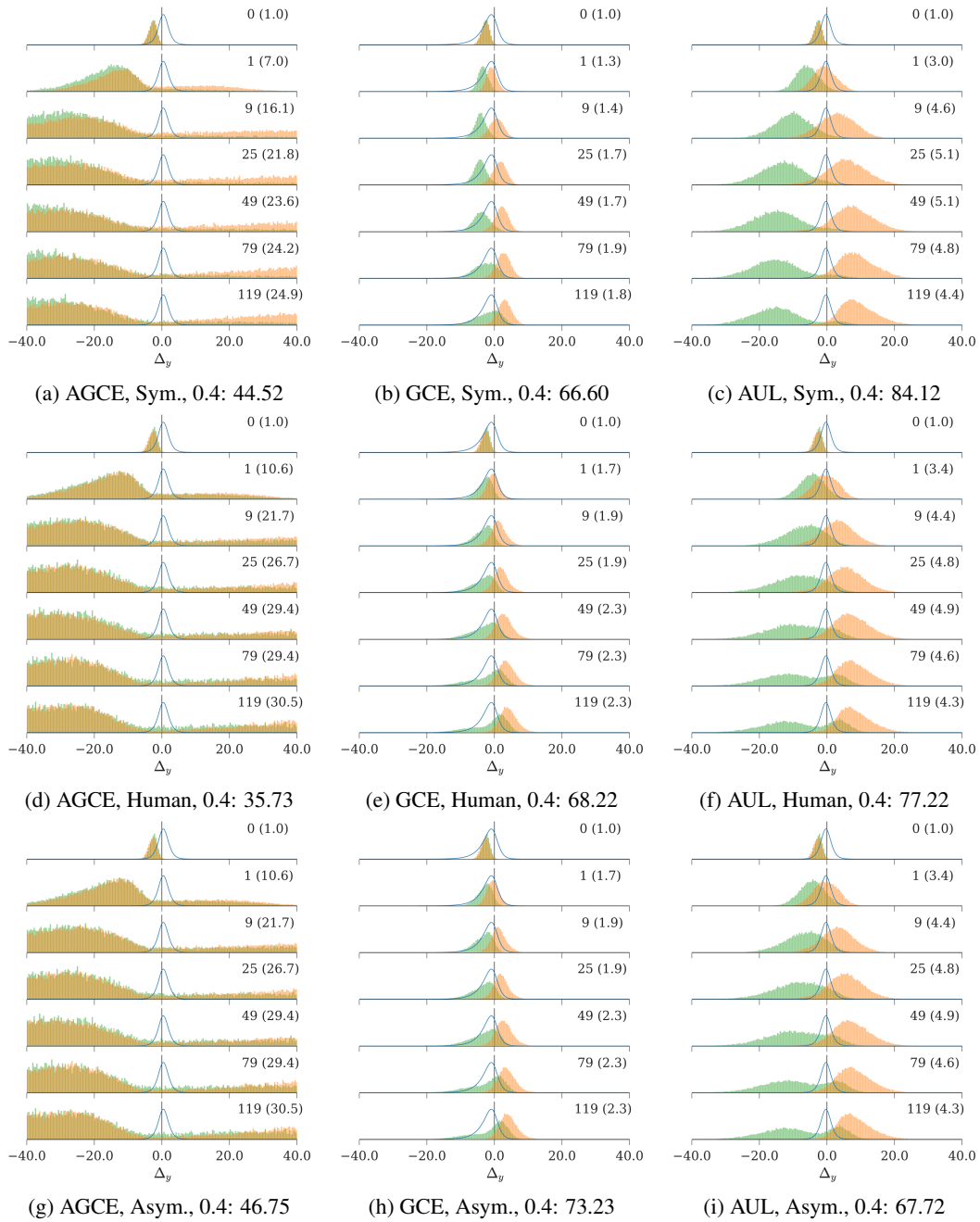


Figure 10: Additional results to Fig. 3 with more robust loss functions under different label noise: (a-c) symmetric label noise with  $\eta = 0.4$ ; (d-f) human label noise with  $\eta = 0.4$ ; (g-i) asymmetric label noise with  $\eta = 0.4$ . Test accuracies are included in the caption for reference. Noisy samples are colored green (on the left) and clean samples are orange (on the right). Hyperparameters of these loss functions are selected for broad coverage rather than optimal performance.